Heliyon 10 (2024) e38494

Contents lists available at ScienceDirect

Heliyon

journal homepage: www.cell.com/heliyon

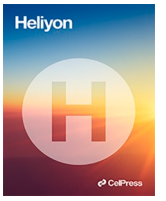

Research article

5-Fluorouracil adsorption on graphene oxide-amine modified graphene oxide/hydroxyapatite composite for drug delivery applications: Optimization and release kinetics studies

Ebru Kahraman *, Gulhayat Nasun-Saygili

Chemical Engineering Department, Istanbul Technical University, 34469, Turkey

ARTICLE INFO

Keywords:
5-Fluorouracil
Hydroxyapatite
Optimization
Drug delivery
Graphene oxide

ABSTRACT

The present study focused on investigation of graphene oxide/hydroxyapatite (GO/HAp) and amine modified graphene oxide/hydroxyapatite (GO-NH_2/HAp) composites as potential drug carrier agents for 5-Fluorouracil (5-FU). Incorporation of 5-Fluorouracil drug was performed via adsorption through π-π interactions and electrostatic attractions. Modification of graphene oxide was performed for the production of amine modified graphene oxide/hydroxyapatite composite with the intention of enhancing adsorption performance. The X-Ray Diffraction (XRD), Fourier Transform Infrared Spectroscopy (FTIR), Thermogravimetric Analysis (TGA) and zeta potential/particle size analysis were performed for particle characterization while Scanning Electron Microscopy (SEM) and Transmission Electron Microscopy (TEM) analysis were used to analyze detailed morphological properties. Experimental design studies were followed out in order to determine the effect of adsorption parameters including graphene oxide amount, pH and initial drug concentration on 5-Fluorouracil adsorption behavior. Adsorption isotherms of both composites with unmodified and modified GO were best fitted to Freundlich model with R^2 values of 0.9616 and 0.9682 respectively. The maximum adsorption capacities (q_m) were calculated as 47.3 mg/g and 18.4 for graphene oxide/hydroxyapatite and amine modified graphene oxide/hydroxyapatite composites respectively at pH 2.0. The highest adsorption percentage was obtained for amine modified graphene oxide/hydroxyapatite composite as 40.87 % at pH 2.0 condition. In vitro release kinetic studies revealed that compliance with Higuchi and Korsmeyer-Peppas kinetic models were observed for graphene oxide/hydroxyapatite, whereas zero order and Korsmeyer-Peppas kinetic models pointed out as the well-fitted model for amine modified graphene oxide/hydroxyapatite composite. The release period of 5-FU drug from all composites were continued up to 8–10 h in physiological conditions (pH 7.4, 37 °C) indicating an achieved controlled release. Based on the overall findings, graphene oxide/hydroxyapatite and amine modified graphene oxide/hydroxyapatite composites could be suggested as a potential drug delivery agent for 5-FU in clinical applications.

1. Introduction

Cancer as one of the most significant causes of mortality has been known to require severe therapy methods including surgery,

* Corresponding author.
E-mail address: kahramaneb@itu.edu.tr (E. Kahraman).

https://doi.org/10.1016/j.heliyon.2024.e38494
Received 25 June 2024; Received in revised form 11 September 2024; Accepted 25 September 2024
Available online 28 September 2024

radiotherapy and chemotherapy [1]. Chemotherapy is one of the traditional methods practiced as a cancer treatment, performed by the administration of highly toxic drugs intravenously [2]. Depending on the kind of utilized anti-cancer agent, the therapeutic efficiency of the treatment could be significantly low, because of the short circulation time through the body and non-selectivity to cancer cells [3]. In order to address these limitations, biomaterials have been proposed in the recent years as drug carriers for providing a controlled release manner. Controlled drug delivery systems have a potential to keep drug concentration within the range of therapeutic window, thus reducing the adverse effects and increasing circulation time [4]. Hydroxyapatite and graphene oxide are among these delivery system constituents which have gained attention as potential drug carriers.

Hydroxyapatite ($Ca_{10}(PO_4)_6(OH)_2$, HAp) is a calcium phosphate bioceramic being one of the basic components of bone tissue. Due to its significant biocompatibility, bioactivity and osteoconductivity, HAp emerges as a highly demanded biomaterial in the fields of dentistry and bone tissue engineering as a filling material and scaffold [5,6]. Apart from that, HAp also has been considered as an appropriate drug carrier material mainly because of its drug adsorption ability and pH responsive behavior [7]. Since nanosized hydroxyapatite particles demonstrate growth-inhibiting effect on cancer cells, hydroxyapatite containing materials could be opted for drug delivery systems of anti-cancer drugs. The calcium ions released from HAp structure has been known to enhance the cancer therapy effectiveness by the disruption of intracellular calcium homeostasis [8]. However, single use of HAp was reported to result in burst release of drug which is undesirable for maintaining controlled delivery [9,10]. The hard and brittle structure of HAp also stands out as a mechanical disadvantage limiting the single use of hydroxyapatite in clinical applications. For these reasons, performance of HAp as a drug delivery agent has been preferred to be enhanced with the contribution of various materials including polymers [11–14] ionic substitutions [15,16] and carbon based [17–19] nanoparticles.

Graphene oxide (GO) is an oxidation derivative of graphene possessing a two-dimensional structure and layered morphology. The molecular structure of GO is decorated with oxygen bearing functional groups such as carboxyl and carbonyl groups at the edge and epoxy groups with hydroxyl on the basal plane. Due to the high specific surface area of GO together with its ability to adsorb drug molecules through hydrogen bonding and π-π interactions, GO have been considered as a potential drug delivery agent candidate in recent years [20,21]. The oxygen containing functional groups provide notable hydrophilic characteristics enhancing dispersibility and stability in physiological conditions, offering a good biocompatibility as a result [22]. However, alone administration of GO reportedly holds potential for a possible decline in the mammalian cell viability, leading to potential toxic activity [23]. In this context, further functionalization of GO for improved features based on intended drug delivery application have been investigated extensively. A wide range of biomaterials have been proposed including chitosan [24], polyethylene glycol [25], gelatin [26], carboxymethyl cellulose [27], polylactic acid [28], β-Cyclodextrin [29] and metal organic framework [30], utilized together with GO. Among these, graphene oxide/hydroxyapatite containing composites also have been investigated for tissue engineering and drug delivery applications as potential drug carrier of ibuprofen [19], amoxicillin [31], vitamin D [32] and doxorubicin [33].

5-Fluorouracil (5-FU) is a commonly used anticancer drug which is an uracil analogue, applied for the treatment of numerous cancer types including skin, breast, colon, stomach, lung, ovarian, head and neck cancers. There is a fluorine atom replaced with hydrogen atom at the C-5 position of 5-Fluorouracil structure and anticancer activity is displayed by thymidylate synthase inhibition [34,35]. The highly toxic characteristic of 5-FU drug for not only cancer cells but also healthy cells results in severe side effects such as hair loss, fatigue, fever and mouth erosions [36,37]. Also, short circulation time through the body (8–20 min) and non-selectivity to cancer cells emerge as limiting factors for therapeutic efficiency of 5-FU. In this regard, providing the controlled release of 5-FU through a carrier is substantial for enhancing the therapeutic efficiency through prolonged circulation time, which in turn increase the likelihood of drug's interaction with cancer cells. To this day, 5-FU incorporated biomaterials have been studied as carriers including HAp and GO such as hydroxyapatite/(poly(lactic-co-glycolic acid)) [38], hydroxyapatite/chitosan [39], graphene oxide/-sodium alginate [40] and graphene oxide/chitosan [41]. Previously published studies on the adsorption behavior of 5-FU drug on various composites have been found in the literature investigated for both drug delivery and drug removal from waste water applications. Compounds including chitosan functionalized graphene oxide [41], chitosan modified single walled carbon nanotube [42] and mesoporous silica SBA-15 [43] have been proposed as potential adsorbent for 5-U applied to be in drug delivery systems. In addition, adsorption behavior of 5-FU onto alginate/geopolymer hybrid beads [44], cellulose nanofibrils [45] and MIL-101-NH_2 (Co/Fe) bi-metal–organic framework [46] materials were studied for efficient 5-FU removal from waste water through adsorption. To the extent of our knowledge, adsorption and release behavior of 5-FU from GO/HAp and amine modified GO/HAp composites have not been investigated previously.

In this study, the potential of GO/HAp and amine modified GO/HAp composites as carriers of 5-FU were aimed to investigate for controlled drug delivery purposes. In this context, production and characterization of GO, HAp, GO/HAp and amine modified GO/HAp were carried out initially followed by the drug adsorption performance studies of aforementioned composites. Firstly, GO was synthesized via Hummers' method and incorporated into HAp structure during production by chemical precipitation. Incorporation of 5-FU drug was performed via adsorption through π-π and electrostatic interactions. In order to optimize the 5-FU adsorption conditions, Box-Behnken experimental design studies were conducted including 3 factors and 3 levels. After defining the optimal conditions for 5-FU adsorption, amine modification of GO was performed prior to composite production with the aim of enhancing the adsorption capacity. In addition, the impact of main adsorption parameters including pH, adsorbent dosage and initial drug concentration was assessed. Adsorption isotherm and kinetic studies were performed to better assess the potential of produced composites in biomedical applications as 5-FU carriers.

2. Materials and methods

2.1. Materials

5-Fluorouracil (≥99 %) was obtained from Sigma Aldrich. Sodium chloride (NaCl), calcium hydroxide ($Ca(OH)_2$, 96 %), ortho-phosphoric acid (H_3PO_4, 85 %), n-butylamine and ethanol were purchased from Merck.

2.2. Synthesis of graphene oxide (GO) and amine modified graphene oxide (GO-NH_2)

GO synthesis was performed according to Hummers Method with minor modifications. Production steps were explained in a previous study [47]. Amine modification of prepared graphene oxide was performed with n-butylamine [48]. Firstly, a GO/distilled water mixture was prepared by dispersing 100 mg of GO in 50 ml distilled water in a beaker and ultrasonicated for 30 min via ultrasonic homogenizer (power: 15 %, pulse mode: 0.6 s on/5 s off). In another beaker, 150 mg n-butylamine and 15 ml ethanol were added and sonicated with ultrasonic bath for 10 min. Then, obtained GO/distilled water and n-butylamine/ethanol mixtures were placed into a flask in an oil bath and allowed to stir at 250 rpm under reflux at 60 °C for 20 h. After the completion of amination reaction, resultant black mixture was left undisturbed for 24 h, followed by separation via centrifugation at 4000 rpm for 20 min. Extracted GO-NH_2 product was washed with ethanol several times with bath sonication and dried overnight at 40 °C in a drying oven.

2.3. Preparation of graphene oxide/hydroxyapatite (GO/HAp) and amine modified graphene oxide/hydroxyapatite (GO-NH_2/HAp) composites

In order to obtain GO/HAp-2 composite with a GO content of %2 (w/w), graphene oxide-distilled water mixture (0.8 mg/ml) was prepared and 25 ml of this mixture was ultrasonicated at 35 °C for 30 min via ultrasonic homogenizer (power: 15 %, pulse mode: 0.6 s on/5 s off). In the meantime, calculated amounts of $Ca(OH)_2$ and H_3PO_4 for 1 g hydroxyapatite production according to Eq. (1) were taken into separate beakers including 50 ml distilled water. After adding the sonicated GO/water to $Ca(OH)_2$/water, resultant mixture was stirred continuously at 37 °C for 1 h together with H_3PO_4 solution at 40 °C. The homogenized H_3PO_4 solution was added dropwise to the aqueous $Ca(OH)_2$/GO mixture by peristaltic pump at a rate of 5 ml/min. After this period, pH was adjusted to be in the range of 9–10 by adding 1 M NaOH solution, if necessary. The final mixture was aged for 24 h, filtered through filter paper, washed with de-ionized water and dried for 24 h at 40 °C in a drying oven. This experimental route was followed similarly by varying the GO content (2.0 mg/ml and 3.2 mg/ml) for production of composites named GO/HAp-5 and GO/HAp-8. For the production of GO-NH_2/HAp composite, GO-NH_2 sample was used instead of GO.

$$10\ Ca(OH)_2 + 6H_3PO_4 \rightarrow Ca_{10}(PO_4)_6(OH)_2 + 18H_2O \quad (1)$$

2.4. Adsorption experiments

Loading of anticancer 5-FU drug onto composites were performed through adsorption based on the experimental design conditions presented in Table 2. Predetermined amount of drug was dissolved in 50 ml distilled water adjusted to selected pH (2, 6 or 10) in a way that 0.02 mg/ml, 0.06 mg/ml and 0.1 mg/ml initial drug concentrations were obtained. Then, 50 mg composite was added, followed by stirring at room temperature at 300 rpm in the dark overnight. After 24 h, 5-FU loaded composite was collected via filter paper and dried in a drying oven for 24 h at 40 °C. This experimental route was conducted for all composites depending on the concentration parameters presented in *2.8. Experimental design* section. Also, various additional adsorbent dosages (25, 75 and 100 mg) and initial drug concentrations (0.2, 0.3, 0.4 and 0.6 mg/ml) were further studied to comment on the effect of these variables.

2.5. Adsorption isotherm experiments

In order to have a better insight on adsorption behavior and capacity of 5-FU on prepared composites, adsorption isotherms were generated according to Freundlich, Langmuir and Dubinin-Radushkevich isotherm models. The nonlinear expression of Langmuir model is presented by Eq. (2) [49–51]:

$$q_e = \frac{q_m k_L c_e}{1 + k_L c_e} \quad (2)$$

with q_m (mg/g) as the maximum adsorption capacity, q_e (mg/g) as the adsorption capacity, k_L (L/mg) as the Langmuir isotherm constant and c_e (mg/L) as the drug concentration at equilibrium. The adsorption capacity q_e (mg/g) is described as follows by Eq. (3):

$$q_e = (c_0 - c_e)V / m \quad (3)$$

in which V(L) the volume adsorption medium, m(g) the mass of composites and c_0 (mg/L) accounts for the initial drug concentration. In addition, the favorableness of the adsorption process is interpreted against separation factor (R_L), which is expressed in Eq. (4):

$$R_L = \frac{1}{1 + k_L c_{0\ max}} \quad (4)$$

where c_{0max} (mg/L) represents the maximum value of initial drug concentration engaged in adsorption experiments. Eq. (5) proposes the Freundlich isotherm model as:

$$q_e = k_F c_e^{1/n} \tag{5}$$

where n is associated with adsorption intensity and k_F (mg/(g(mg/L)$^{1/n}$)) model constant with adsorption capacity [49,52]. Dubinin-Radushkevich model is represented by Eq. (6) as follows:

$$q_e = q_D e^{\left(-k_D \varepsilon^2\right)} \tag{6}$$

where k_D (mol^2/J^2) stands for the average free energy per mole of adsorbate, q_D (mg/g) the saturation capacity and ϵ (kJ/mol) the adsorption potential expressed in Eq. (7):

$$\varepsilon = RT\ln\left[1 + \left(1/c_e\right)\right] \tag{7}$$

The adsorption free energy calculated in Eq. (8) enables to have an opinion on adsorption nature in regards to being chemisorption, physisorption or ion exchange [49,53].

$$E = 1/\sqrt{2k_D} \tag{8}$$

In order to interpret the compatibility of adsorption isotherm models, Akaike's information criterion (AIC) (Eq. (9), Eq. (10)) and root mean square error (RMSE) (Eq. (11)) values of the models were calculated and compared. The N value represented the number of experimental data, SSE the sum of squares error, N_p the number of parameters, $q_{e,exp}$ experimental drug release (mg/g) and $q_{e,pre}$ predicted drug release (mg/g) from the model equation [54,55].

$$AIC = N\ln\left(\frac{SSE}{N}\right) + 2N_p + \frac{2N_p\left(N_p+1\right)}{N - N_p - 1} \tag{9}$$

$$SSE = \sum_{N=0}^{N}\left(q_{e,exp} - q_{e,pre}\right)^2 \tag{10}$$

$$RMSE = \sqrt{\frac{1}{N}\sum_{N=0}^{N}\left(q_{e,exp} - q_{e,pre}\right)^2} \tag{11}$$

2.6. Drug release studies

In the context of drug release studies, following procedure was performed. Firstly, 10 mg amount of 5-FU loaded composite was inserted into a piece of dialysis tubing (Sigma, 14 kDa) including 5 ml of phosphate buffer solution (PBS) with a pH value of 7.4, the

Table 1
Mathematical models for drug release kinetics studies [56–60].

Model	Equation	Variables and constants
Zero order	$c_t = c_0 + k_0 t$	t: Time (hour) c_0: Initial drug concentration c_t: Released drug amount after the time t k_0: Zero order model constant
First order	$\frac{q_1}{q_0} = e^{-k_1 t}$	t: Time (hour) q_0: Initial mount of drug dissolved q_1: Released drug amount after the time t k_1: First order model constant
Korsmeyer-Peppas	$M_i/M_\infty = kt^n$	t: Time (hour) M_∞: Drug amount at equilibrium M_i: Released drug amount after the time t k: Constant of incorporation n: Release exponent
Higuchi	$q = k_H\sqrt{t}$	t: Time (hour) k_H: Higuchi release constant q: Released drug amount after the time t
Hixson-Crowell	$\sqrt[1/3]{W_0} = \sqrt[1/3]{W_i} + k_{HC}t$	t: Time (hour) W_0: Initial drug amount in the system W_i: Remaining drug amount in the system k_{HC}: Constant of incorporation

edge of the tubing was sealed tightly and placed in a beaker including 100 ml of PBS. The beaker was transferred to a shaking water bath at 120 rpm and 37 °C. At determined time intervals, PBS specimen was collected for analyzing the drug content via ultraviolet–visible (UV–vis) spectrophotometer (Hach DR6000) at 266 nm. Same experimental procedure was conducted also for varied pH values (1.2 and 5.0), composites types and drug loaded composites in adsorption mediums with various initial drug concentrations (0.1, 0.2, 0.3, 0.4, 0.6 mg/ml).

2.7. Drug release kinetics

In order to provide a better insight on drug release kinetics behavior of obtained composites, mathematical models were taken into consideration as of zero-order, first-order, Higuchi, Korsmeyer-Peppas and Hixson-Crowell. Calculated correlation coefficients (R^2) of utilized models were compared and model displaying the highest R^2 value was admitted to be the best fitting model. AIC and RMSE values were also calculated according to Eqs. (9)–(11) as given in *2.5. Adsorption isotherm experiments* section with $q_{e,exp}$ representing the experimental drug release percentage and $q_{e,pre}$ predicted drug release percentage. Referent model equations with variables and constants were described in Table 1.

2.8. Experimental design

Optimum conditions for 5-FU release from GO/HAp composites were determined via Box-Behnken design experiments including 3 factors and 3 levels. Designated design factors including GO amount (% (w/w)), initial drug concentration (mg/ml) and pH as the independent variables at different levels were given in Table 2. Amount of adsorbed drug (%(w/w)) (y_1) values obtained from experimental data assigned as the designed experiment response which is also the dependent variable. A number of 15 experimental runs with 3 center points were required by the design experiment, from which a second order polynomial was evaluated via Minitab 21 Software. Contour plots were obtained via Design Expert Software.

Analysis of variance (ANOVA) calculations were investigated to understand significance of the selected independent variables (p-value<0.05) and relevancy of the model was interpreted considering R^2 and adjusted R^2 values. Created three-dimensional surface and contour plots were referred to examine individual and bilateral interactions of the variables. The formulation demonstrating the highest response was deduced as the optimum formulation.

2.9. Characterization

XRD analysis was performed with $CuK_{\alpha 1}$ radiation ($\lambda = 1.5406$ Å) for 2θ ranging from 10° to 80° (PANalytical X'Pert PRO). FTIR analysis of obtained products were carried out via PerkinElmer Spectrum 100 FTIR spectrophotometer covering the region 650–4000 cm^{-1}. The effect of GO incorporation to HAp structure on thermal behavior was investigated by TGA performed with PerkinElmer Diamond TG/DTA by heating with a rate of 10 °C/min (25–550 °C) under nitrogen atmosphere. The particle size measurements were carried out by dynamic light scattering (DLS) method together with zeta potential measurements by Malvern Zetasizer Nano ZS. The surface morphologies were investigated by use of SEM operated at 10 KV (SEM, Zeiss EVO® LS 10). Detailed morphological structures were examined through transmission electron microscopy (TEM) (JEOL JEM-1400 PLUS). Stability of the produced composites were assessed by wavelength scanning in the range of 250–600 nm via (UV–vis) spectrophotometer (Hach DR6000).

3. Results and discussions

3.1. XRD

XRD patterns of GO, HAp, GO/HAp and GO-NH_2/HAp composites are presented in Fig. 1. The peak at $2\theta = 10.56°$ in GO diffraction pattern was detected as the characteristic peak of GO confirming the successful oxidation process of graphite [25,61]. The appearance of diffraction peaks at $2\theta = 25.92°$, 31.83°, 32.08°, 39.79°, 46.79° and 49.50° showed that characteristic peaks of HAp phase were present, confirming the formation of HAp structure in the composites [62]. As the main phase of the composites are HAp, no significant change from HAp was detected for GO/HAp and GO-NH_2/HAp composites as expected, while all the characteristic HAp diffraction peaks were present a s well.

Table 2
Independent and dependent variables of designed Box-Behnken experiments.

Factors/independent variables		Levels		
		Low (−1)	Medium (0)	High (1)
GO amount (%(w/w))	$\mathbf{x_1}$	2	5	8
Initial drug concentration (mg/ml)	$\mathbf{x_2}$	0.02	0.06	0.10
pH	$\mathbf{x_3}$	2	6	10

Dependent variable $\mathbf{y_1}$ = Amount of adsorbed drug (%(w/w)).

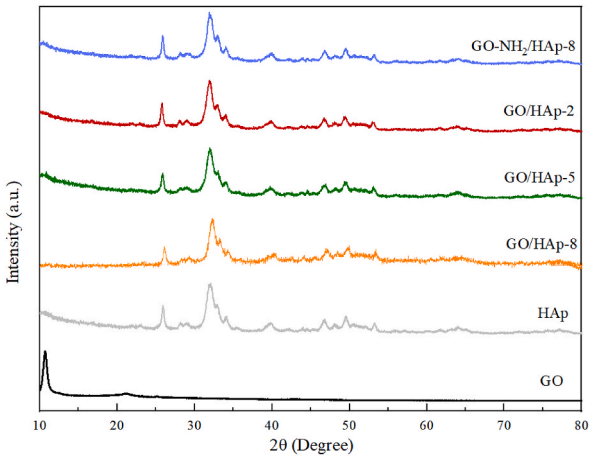

Fig. 1. XRD patterns of GO, HAp, GO/HAp and GO-NH_2/HAp.

3.2. FTIR

FTIR spectra of GO/HAp composites and 5-FU loaded GO/HAp-8 are given in Fig. 2 in comparison with GO. The disappearance of the C=O absorption band peaks at 1720 cm^{-1} belonging to the carboxyl groups of GO structure confirmed the formation of covalent bonds with Ca^{2+}, which was indicative of the strong interaction between HAp and GO [63,64]. At 1023 cm^{-1} (ν3), P-O asymmetric stretching vibrations belonging to PO_4^{-3} groups as one of the characteristic peaks of HAp were determined in all composite samples. In addition, P-O symmetric stretching vibrations corresponding to PO_4^{-3} groups were observed at 963 cm^{-1} (ν1). The peaks emerged at

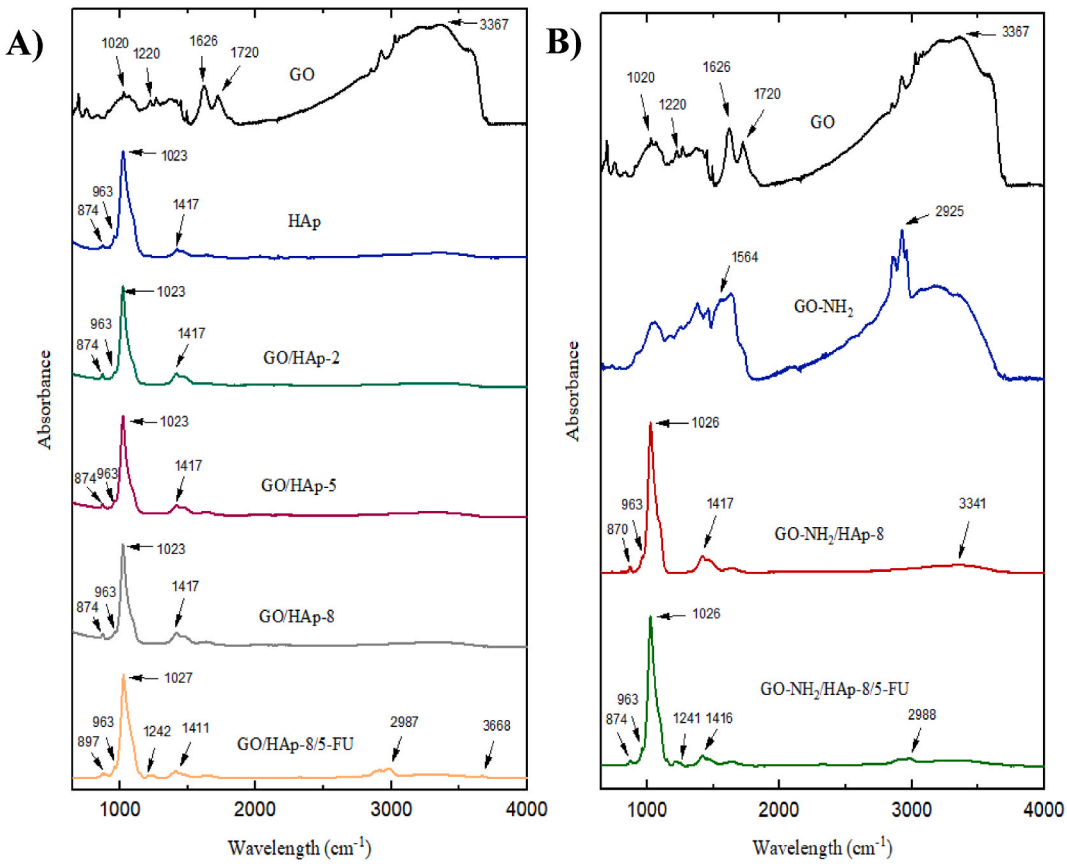

Fig. 2. FTIR spectra of A) GO, HAp, GO/HAP and 5-FU loaded GO/HAp composite, B) GO, GO-NH_2, GO-NH_2/HAp and 5-FU loaded GO-NH_2/HAp composite.

1417 cm^{-1} ($\nu 3$) and 874 cm^{-1} ($\nu 2$) appeared to originate from CO_3^{-2} ions present in the HAp structure [65]. Also, the peaks at 874 cm^{-1} pointed out the participation of carbonate ions to OH^- containing regions during synthesis. The FTIR spectra GO/HAp samples did not reveal a significant difference in comparison with HAp, possibly the result of small GO amounts present in composites. In case of modified GO-NH_2 sample, two distinct peaks at 2925 cm^{-1} and 2956 cm^{-1} emerged after amine functionalization, representing the stretching vibrations of C-H originating from aliphatic chains of amines [66]. The peak observed at 1564 cm^{-1} was the characteristic peak indicating the presence of in-plane N-H [67]. The intensity of the broad peak of OH stretching vibration between 3000 and 3400 cm^{-1} in GO spectra decreased and peak at 1720 cm^{-1} corresponding to carboxyl groups completely disappeared after functionalization. This could be interpreted as the amine modification of GO was performed successfully [66]. The peak observed around 1240 cm^{-1} in drug loaded GO/HAP-8 and GO-NH_2/HAp composites was ascribed to the existence of characteristic C-N vibrations of 5-FU [68]. In addition, peak at 897 cm^{-1} corresponding to C-C stretching, peak at 2987 and 2988 cm^{-1} representing C-H asymmetric stretching and peak at 3668 cm^{-1} indicating O-H and C-H stretching were attributed to the presence of 5-FU [69]. In summary, the FTIR study confirmed the formation of composites and successful adsorption of 5-FU drug.

3.3. TGA

TGA analysis of GO/HAp and GO-NH_2/HAp composites were carried out in order to investigate the effect of GO content and amine modification on the thermal stability of composites. As observed from Fig. 3A, plain HAp exhibited a high thermal stability with an approximately 9 % weight loss at 550 °C. Meanwhile, decomposition of GO and GO-NH_2 incorporated composites occurred in two stages with a slightly higher final weight loss in comparison with HAp. The first stage of decomposition indicated to the evaporation of water molecules until around 125 °C for all samples. While the second stage between 125 and 325 °C could be ascribed to the pyrolysis of functional groups within GO structure. A slight relapse of thermal stability was observed as the contents of GO were increased, with an approximately 14 % final weight loss for the highest GO content of 8 %. This could be associated with the increase in mass loss due to pyrolysis of oxygen bearing functional groups in the composite structure as the amount of GO increases [31,70]. Amine modification of GO resulted in accelerated weight loss up to 200 °C, possibly due to the additional weight loss by the elimination of covalently bonded n-butylamine within GO-NH_2 structure [66]. From 200 °C up until 550 °C, TGA curves of GO/HAp-8 and GO-NH_2/HAp-8 overlapped as expected, simply because involving similar amount of oxygen containing functional groups. The two-staged degradation of GO and GO-NH_2 incorporated composites could also be observed in DTG analysis (Fig. 3B). It is a known fact that increase in the area under the DTG curve denotes higher mass loss. Considering the areas under the DTG curves around 120 °C, it is clear that higher GO and GO-NH_2 content inclined an increase in the mass loss meaning the thermal stability of HAp slightly regressed.

3.4. Zeta potential and particle size distribution

Particle size distribution of GO/HAp-8 and GO-NH_2/HAp-8 composites are presented in Fig. 4. GO/HAp-8 composite showed a size distribution in the range of 10–300 μm, with a maximum of 248.9 μm and average particle size of 118.3 μm (Fig. 4A). While GO-NH_2/HAp-8 composite also showed a size distribution within the same range with a maximum of 292 μm, the average particle size was obtained as 155.2 μm (Fig. 4B). From zeta potential measurements (Table 3), an increase in the negative surface charge of HAp with the incorporation of GO was detected, from −1.7 mV to maximum of −14.7, corresponding to the presence of negatively charged carboxyl groups in GO structure. Whereas, GO/HAp composites exhibited quite lower surface charge values in comparison with GO, possibly the

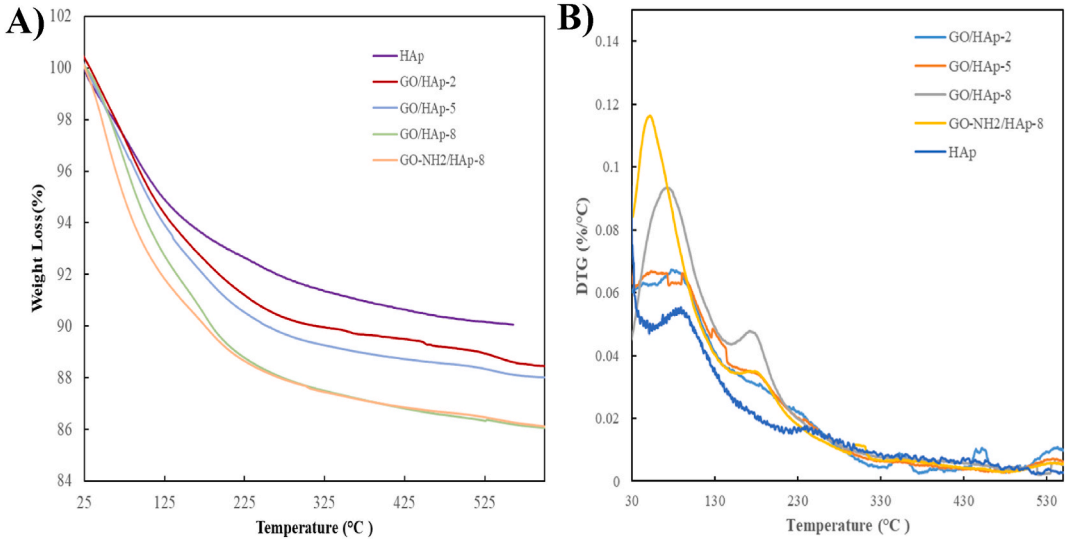

Fig. 3. A) TGA and B) DTG curves of HAp, GO/HAp-2, GO/HAp-5, GO/HAp-8 and GO-NH_2/HAp-8.

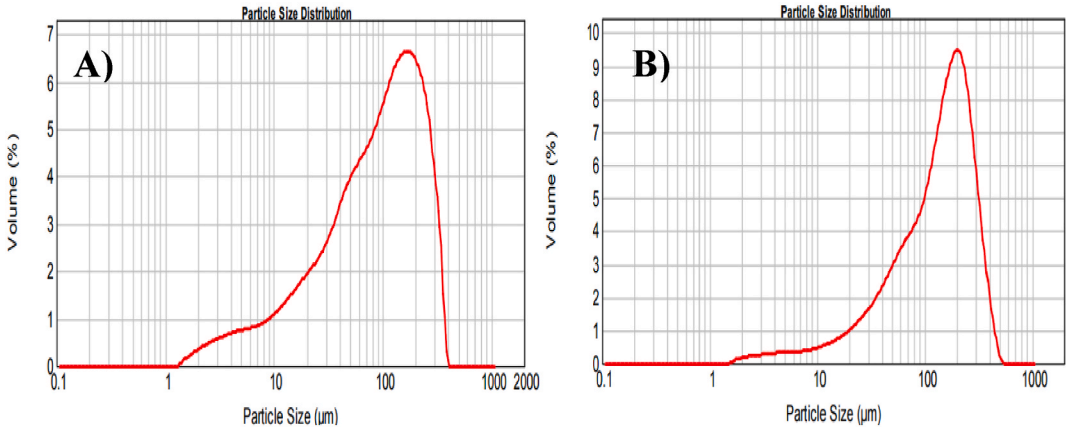

Fig. 4. DLS measurements of A) GO/HAP-8, B) GO-NH_2/HAp-8 composites in aqueous solution.

Table 3
Zeta potential measurements.

Sample	Zeta Potential (mV)
GO	−39.6
HAp	−1.7
GO-NH_2	−31.8
GO/HAp-2	−0.74
GO/HAp-5	−14.7
GO/HAp-8	−10.8
GO-NH_2/HAp-8	12.7

result of the composite formation mechanism. During production process, oxygen containing functional groups existed on GO surface including hydroxyl, epoxy and carboxyl, acted as nucleation sites for HAp crystals to be formed. This process induced by the attachment of Ca^{2+} ions on negatively charged functional groups of GO or through ion exchange with H^+ ions of carboxyl groups. Following the attachment of Ca^{2+} ions on GO surface, negatively charged PO_4^{3-} and OH^- ions existed in the aqueous medium were attracted by Ca^{2+} ions, which in turn initiated the formation of HAp crystals on GO surface [62]. Therefore, the drop in the negative surface charge values could be explained by the participation of negatively charged functional groups to HAp crystal formation. In addition, relatively lower amounts of GO in comparison to HAp might have resulted in closer surface charge values to HAp. In contrast with GO/HAp, GO-NH_2/HAp composite revealed a positive surface charge, possibly the result of NH_2 groups contribution. It is a known fact that protonation of NH_2 groups results in the formation of NH_4^+ ions, providing a positive surface charge [71]. In case of GO-NH_2, a negative surface charge close to GO might have been obtained as the negatively charged oxygen containing functional groups outnumbered the NH_2 groups. While for GO-NH_2/HAp, the number of carboxyl and other functional groups on GO-NH_2 surface could have reduced upon HAp crystal formation, leading to positive charge domination originated from NH_2 groups contribution. Hence, it can be suggested that NH_2 groups emerged as the distinctive factor for the surface charge value of the composite.

3.5. SEM

The surface morphologies of produced samples and drug loaded composites were examined by SEM images presented in Fig. 5. A sponge like morphology was detected for HAp powder, which is a reported characteristic of chemical precipitation method based HAp products obtained with H_3PO_4 as a phosphate source [72,73]. The smooth and sheet like surface of GO was found to be rougher following HAp crystal growth, resulting in a similar sponge like structure in comparison with HAp alone. The GO/HAp composites with adsorbed 5-FU on its surface displayed a smoother surface compared to GO/HAp, showing a decrease in its sponge like structure. This could be associated with the release of Ca^{2+} and PO_4^{3-} ions from the HAp surface to the aqueous adsorption medium. Composites with amine modified GO also exhibited a smoother surface in comparison with GO/HAp composite, lacking of the sponge like morphology of HAp sample. Possible explanation could be the declining of oxygen containing functional groups upon amine modification, which in turn leaving less nucleation sites for HAp growth. Hence, rough and sponge like morphology of HAp might not be obtained.

3.6. TEM

In order to observe the detailed morphology of GO, HAp, GO/HAp and GO-NH_2/HAp sample structures, TEM analysis was performed and images were presented in Fig. 6. A sheet like and wrinkled morphology for GO was detected similar to reported studies in literature [74,75] whereas elongated crystal morphology was observed for HAp [76]. The nucleation and deposition of HAp particles

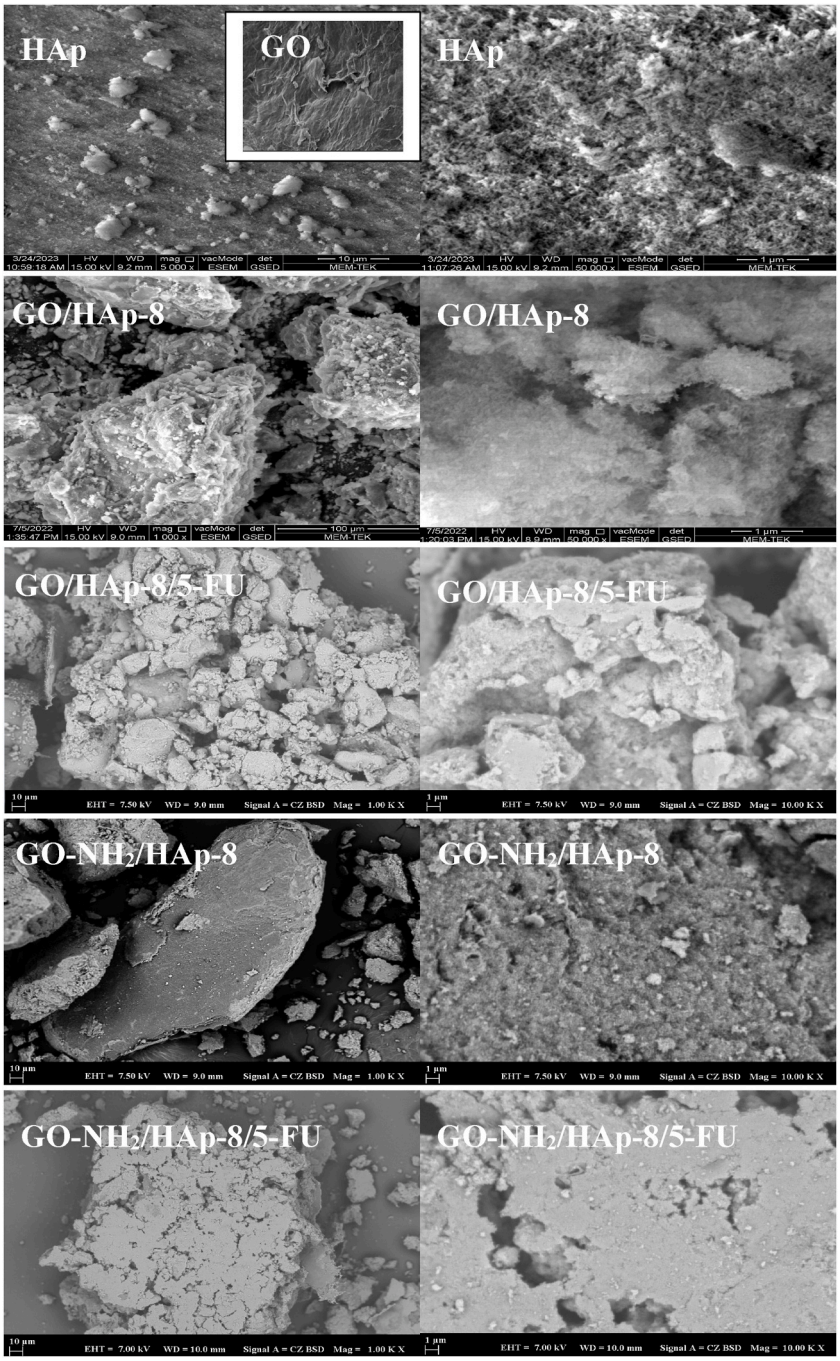

Fig. 5. SEM images of HAp, GO, GO/HAp-8, GO/HAp-8/5-FU, GO-NH_2/HAp-8, GO-NH_2/HAp-8/5-FU.

on GO planar sheet were clearly demonstrated by the images of GO/HAp-8 sample, where HAp particles were appeared as darker elongated structures [77]. Similar morphology was also observed for GO-NH_2/HAp-8 composite, confirming the HAp crystal formation on amine modified GO planar surface.

3.7. Stability

The stability of produced GO/HAp-8 and GO-NH_2/HAp-8 composites in the water as an adsorption medium were examined by absorbance measurements at pH values of 2, 4 and 6 (Fig. 7). Composites were stirred for 24 h as in the adsorption experiments and samples were taken for absorbance measurements at predetermined time intervals. For both GO/HAp-8 and GO-NH_2/HAp-8

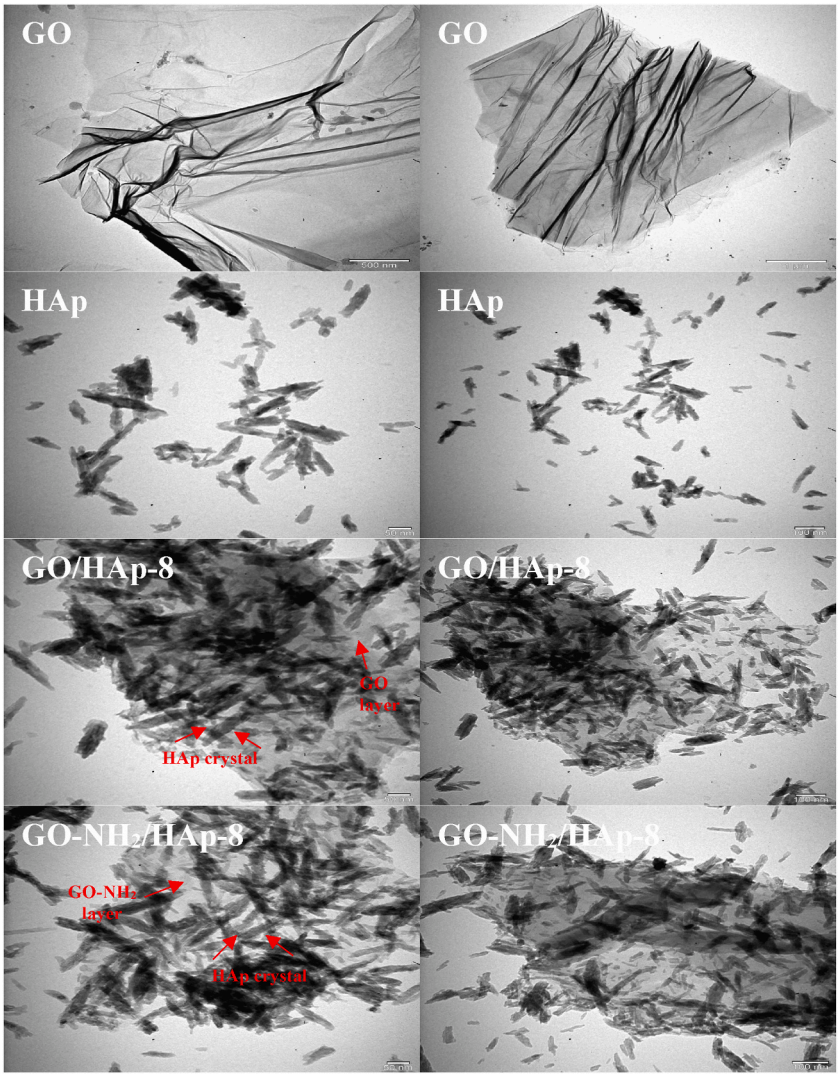

Fig. 6. TEM images of HAp, GO, GO/HAp-8 and GO-NH_2/HAp-8.

composites, an increase in the absorption strength was detected after 6 h for all pH values. This could be associated with better homogenization of the composite particles with increasing agitation time, leading to absorbance increase. Meanwhile, lowest absorption values were observed after 24 h for GO/HAp-8 composite at pH 2 and 6, indicating slightly loss of stability for these conditions with time. No significant change in the absorption spectra was occurred with time and pH change, eliminating the possibility of composite decomposition [78,79].

3.8. Experimental design and optimization studies of GO/HAp

The obtained data from experimental design studies are presented in Table 4 including experimental and predicted adsorbed 5-FU percentages. The maximum adsorption percentage was determined as 26.3 % (R6) whereas minimum adsorption was 5.5 % (R8). The ANOVA Table (Table 5) was generated considering the elimination of insignificant terms and a quadratic mathematical expression for the adsorption of 5-FU on GO/HAP was obtained (Eq. (9)). The integrity of the data was confirmed with a R^2 value 91.91 % and an adjusted R^2 of 88.67 %. The ANOVA results revealed a p value below 0.05 together with a lack of fit value higher than 0.05 ($p = 0.196$, $F = 4.47$), notating an acceptable significance level.

The influence of independent variables on drug adsorption and their bilateral interactions were assessed via contour plots and are presented in Fig. 8. As observed from Fig. 8A and B, highest adsorption was tended to occur in case of high GO amount and low initial 5-FU concentrations. While elevating GO incorporation did not make a significant difference at a fixed initial concentration of 5-FU, increasing the initial concentration at a fixed amount of GO significantly reduced the adsorption percentage. Similarly, in Fig. 8C and D, increasing the pH value at constant amount of GO resulted in lower adsorption percentages. While Fig. 8E and F indicated highest

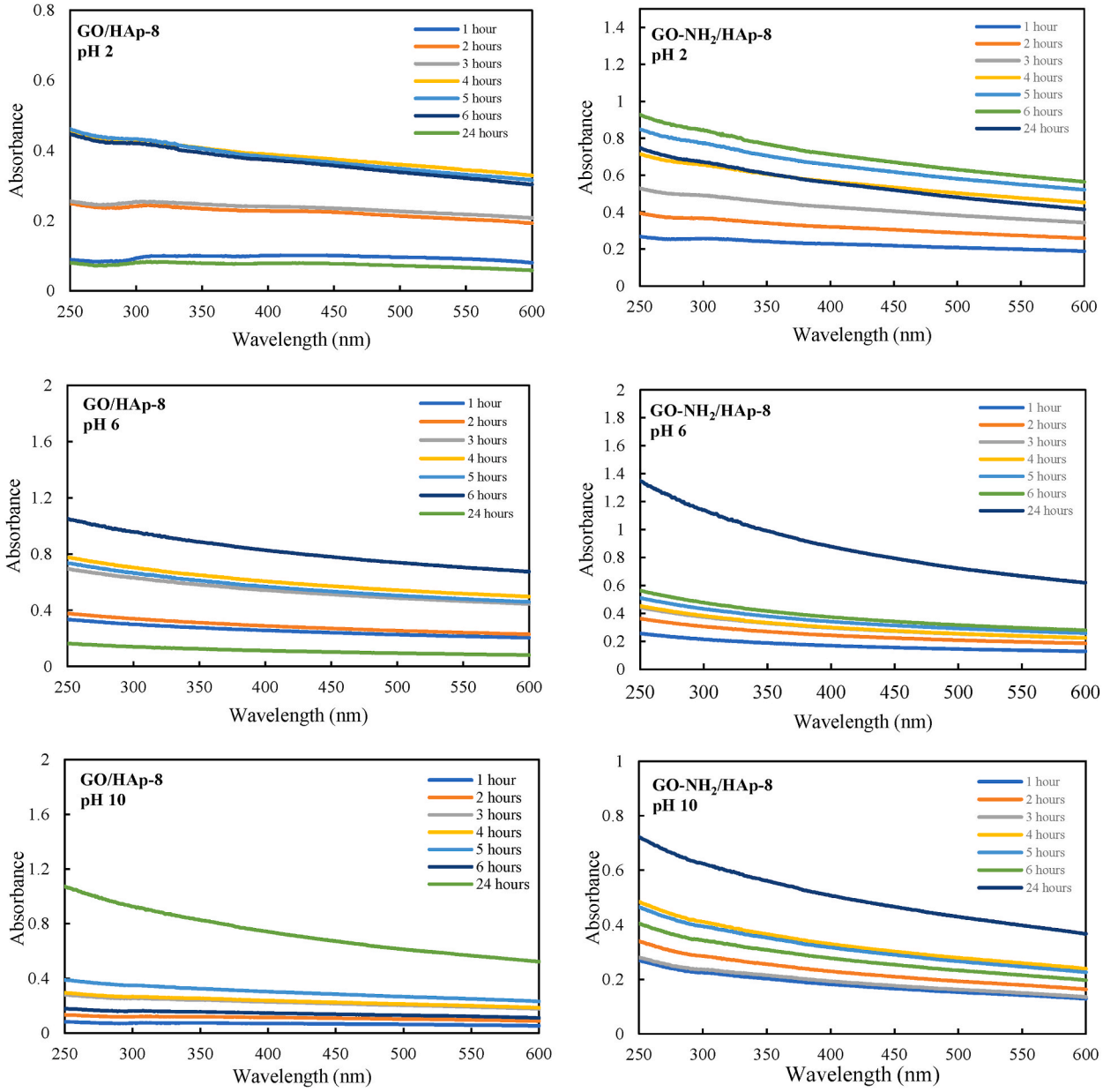

Fig. 7. UV–Vis spectrum of the GO/HAp-8 and GO-NH_2/HAp-8 composites in water medium.

adsorption performance at low pH and initial 5-FU concentrations. Considering the coefficients of the model equation, initial 5-FU concentration emerged as the most prominent factor due to the highest absolute value. Overall data demonstrated that a significant increase in drug adsorption percentage at low pH levels and 5-FU initial concentrations were observed, while the increase in the amount of GO leaded to a slight increase being the factor with the lowest effect. Experimental values in comparison with predicted values of the adsorbed percentages of drug obtained from Box-Behnken design were depicted in Fig. 8G. Based on the obtained results, adsorption experiment was repeated under the conditions expected to give the best results (pH 2, GO: 8 %, initial drug concentration: 0.02 mg/ml). Since these conditions were not included in the planned experimental design, they were also accepted as an experiment to verify the obtained model equality. Under these conditions, the percentage of adsorbed drug was obtained as 31.19 %, while the value calculated using the model equation was 29.89 %. Hence, aforementioned implication for the highest drug adsorption conditions were confirmed. Adsorption of 5-FU molecules on GO/HAp composite corresponds to the hydrogen bonds with GO functional moieties, π-π interactions with aromatic groups of GO and electrostatic interactions with HAp surface. Consequently, increasing amount of GO incorporation might have resulted in larger number of available functional and aromatic groups for 5-FU to interact, which in turn improved adsorption. A possible elevation in the HAp surface area at low pH values was reported in literature previously, which was

Table 4
Predicted adsorption data of GO/HAp by Box-Behnken design with design points and experimental data.

Runs	Parameters			Responses	
	x_1	x_2	x_3	y_1	
				Experimental	Predicted
R1	2	0.06	2	18.47	19.27
R2	5	0.06	6	12.98	13.16
R3	5	0.06	6	10.39	13.16
R4	2	0.02	6	24.41	22.06
R5	2	0.10	6	5.66	6.60
R6	8	0.02	6	26.34	24.91
R7	8	0.10	6	6.43	9.46
R8	5	0.10	10	5.46	0.48
R9	5	0.02	10	14.72	15.94
R10	5	0.10	2	11.47	10.37
R11	5	0.06	6	11.69	13.16
R12	8	0.06	2	24.60	22.13
R13	2	0.06	10	8.78	9.38
R14	5	0.02	2	25.37	25.83
R15	8	0.06	10	11.36	12.24

x_1 = GO amount (%(w/w)); $\mathbf{x_2}$ = Initial drug concentration (mg/ml); $\mathbf{x_3}$=pH; y_1 = Amount of adsorbed drug (%(w/w)).

Table 5
ANOVA calculations for GO/HAp adsorption data.

Source	DF	Adj SS	Adj MS	F-Value	P-Value
Model	4	715.201	178.8	28.39	**0.000**
Linear	3	689.948	229.983	36.51	0.000
$\mathbf{x_1}$	1	16.325	16.325	2.59	0.139
$\mathbf{x_2}$	1	477.821	477.821	75.86	0.000
$\mathbf{x_3}$	1	195.802	195.802	31.09	0.000
Square	1	25.253	25.253	4.01	0.073
$\mathbf{x_1{*}x_1}$	1	25.253	25.253	4.01	0.073
Error	10	62.988	6.299		
Lack-of-Fit	8	59.653	7.457	4.47	**0.196**
Pure Error	2	3.335	1.667		
Total	14	778.189			

attributed to low OH concentrations at low pH mediums. OH ions presence is required for an effective HAp crystal formation and growth. As high pH value mediums prone to bear higher OH concentrations, increasing pH value of adsorption medium might have caused further crystal formation during adsorption, leading to surface area reduction through agglomeration [80]. Accordingly, surface area increment at low pH values could potentially enable 5-FU adsorption and led to considerably high adsorption percentages.

$$\mathbf{y_1} = 13.155 + 1.428\ x_1 - 7.728\ x_2 - 4.947\ x_3 + 2.60 \times 1 \times {}_1 \quad (9)$$

3.9. Adsorption experiments after amine modification

In order to investigate the effect of amine modification on 5-FU adsorption, studies at selected experimental design pH values (pH 2, 6 and 10) were conducted for GO-NH_2/HAp composite. The ratio of GO-NH_2 was selected as 8 % since GO/HAp-8 was the composite with highest adsorption efficiency in experimental design studies. Table 6 presents the adsorption percentages of 5-FU onto GO/HAp and GO-NH_2/HAp comparatively. At first glance, almost 10 % increase in 5-FU adsorption could be detected for the adsorption medium pH of 2 and 6, whereas highest adsorption was obtained as 40.87 %. The improvement in 5-FU adsorption following amine modification could be attributed to hydrogen bonds formed between N atoms of amine groups in GO-NH_2/HAp structure and H atoms of 5-FU molecules [81]. While the 5-FU adsorption onto GO/HAP solely occurred through GO functional groups, π-π interactions between aromatic groups and electrostatic interactions on HAp surface; amine modification might have provided additional adsorption sites for 5-FU drug to attach in GO-NH_2/HAp. Similar to GO/HAp, adsorption at increasing pH values also limited 5-FU adsorption onto GO-NH_2/HAp, resulting in percentages as low as 14.72 %. The fact that 5-FU drug has a pKa value in the range of 7.6 and 8.05 [82,83] might have an effect on the adsorption decrease at elevated pH values. 5-FU bear two available deprotonation regions on the N1 and N3 nitrogen of amide in its molecular structure, hence can be found in two anionic figurations above its pKA values [84]. As GO/HAp-8 composite was found to be negatively charged from zeta potential measurements, a possible electrostatic repulsion between GO/HAp-8 composite and negatively charged 5-FU molecules at pH 10 could be suggested as the cause of lower adsorption values. On the contrary, similar adsorption drop was also observed for GO-NH_2/HAp-8 even though its being positively

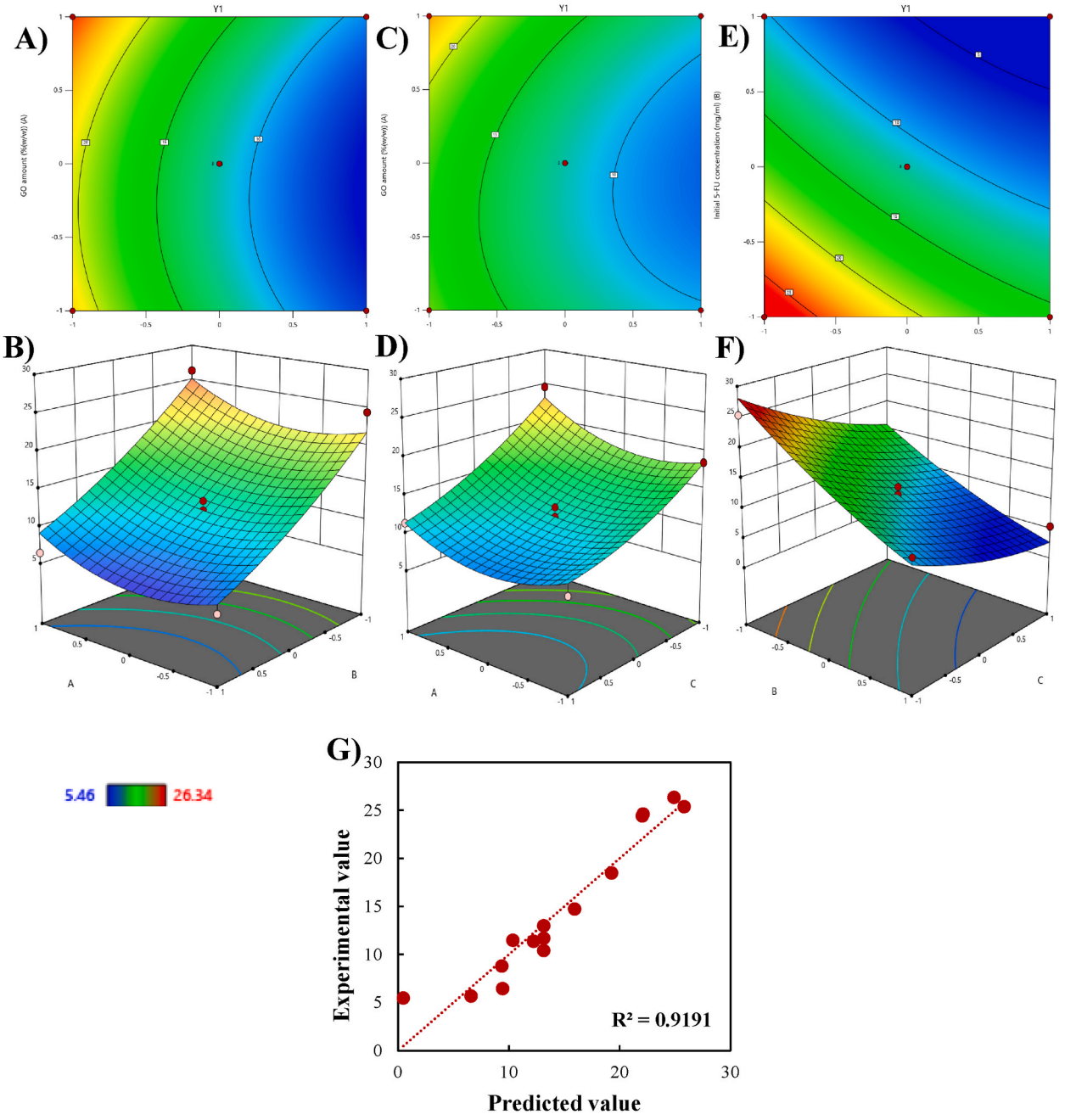

Fig. 8. Three dimensional surface plots and contour plots obtained from experimental design calculations for GO/HAp (A: GO amount (%(w/w)), B: initial drug concentration (mg/ml), C: pH, y_1: amount of adsorbed drug), A-B) GO amount (%(w/w)) vs. initial drug concentration (mg/ml), C-D) GO amount (%(w/w)) vs. pH, E-F) initial drug concentration vs. pH, G) experimental values vs. predicted values.

Table 6
Comparative 5-FU adsorption percentages of GO/HAp-8 and GO-NH_2/HAp-8.

	pH	GO-NH_2/HAp-8	GO/HAp-8
Amount of adsorbed drug ((w/w)%)	2	**40.87**	31.19
	6	37.96	26.34
	10	14.72	19.99[a]

[a] Amount of adsorbed drug ((w/w)%) onto GO/HAP-8 at pH 10 was calculated from model equation obtained in experimental design studies.

charged and higher electrostatic attraction between composite and negatively charged 5-FU molecules was expected. Therefore, electrostatic forces could not be suggested as the dominant factors effecting the adsorption behavior at varying pH values.

3.10. Adsorption isotherms

3.10.1. Adsorption isotherms of GO/HAp composites

Adsorption isotherms of GO/HAp were evaluated against three models including Freundlich, Langmuir, and Dubinin-Radushkevich. Experimental conditions were maintained by selecting the sample with the highest drug adsorption capacity (GO/HAp-8) and the pH value with the highest efficiency (pH 2). For this selected sample, experiments were carried out with different initial drug concentrations in pH 2 environment. Evaluated adsorption isotherm parameters and regression coefficients (R^2) are given in Table 7. Non-linear and linear fit of isotherm models are given in Fig. 9 and Fig. S1 respectively.

Freundlich model emerged as the best fit for 5-FU adsorption on GO/HAp, with the highest R^2 value of 0.9616 together with the lowest RMSE and AIC values. Affinity to Freundlich model could be interpreted as adsorbent GO/HAp's surface is heterogeneous and adsorption is multilayer [85]. From Langmuir model, maximum adsorption capacity (q_m) was obtained as 47.3 mg/g together with a separation factor (R_L) of 0.5330, and n value of 1.8936 from Freundlich model. Both R_L and n values could provide a better insight of the favorability of adsorption process. A R_L value of 0 is associated with an irreversible, R_L value in the range of 0 and 1 favorable, and R_L value > 1 unfavorable adsorption. Whereas 1/n value in the range of 0.2 and 0.8 together with n value between 1 and 10 and is an evidence of good adsorption [49]. Hence, obtained R_L and n values indicated that 5-FU adsorption of GO/HAp was favorable. The free energy of adsorption (E) was determined as 9.28 kJ/mol from Dubinin-Radushkevich model, implying an endothermic adsorption process due to positive E value [49,86]. E value below 8 kJ/mol demonstrates that adsorption occurs by physisorption, E value in the range of 8 and 16 kJ/mol by ion exchange and E value above 16 kJ/mol by chemisorption [49,87]. Therefore, an E value of 50 kJ/mol signified the nature of adsorption on GO/HAp composite was ion exchange. In addition, k_D value was obtained as 0.0058 mol^2/J^2 (<1) from Dubinin-Radushkevich model, which is also an indication of microporous adsorbent surface [49].

3.10.2. Adsorption isotherms of GO-NH_2/HAp composites

Adsorption isotherms of GO-NH_2/HAp were generated under the identical experimental conditions explained in section *3.7.1. Adsorption isotherms of GO/HAp composites* and presented in Fig. 8. Non-linear fits of isotherm models were given in Fig. 10 together with derived parameters in Table 8. Linear fittings of the models were presented in Fig. S2.

Evaluated adsorption isotherm data revealed the maximum adsorption capacity of GO-NH_2/HAp composite as 18.4 mg/g. Similar to GO/HAp composite, the highest compatibility was obtained for Freundlich model with a R^2 value of 0.9682, along with the lowest RMSE and AIC values. The n value from Freundlich model obtained as 4.5364 and 1/n as 0.2204, indicating a favorable adsorption process. In addition, calculated R_L from Langmuir (0.0282) depicted a favorable adsorption process also, as satisfying the condition of $0< R_L < 1$. The E value of Dubinin-Radushkevich model which was calculated as 33.71 kJ/mol, demonstrated an endothermic adsorption process through chemisorption ($E > 16$ kJ/mol). Lastly, a k_D value of 0.00044 mol^2/J^2 signified that composite's surface was microporous.

A summary of adsorption capacities obtained for various materials in recent literature studies was presented in Table 9. While a direct comparison between the adsorption capacities would not be accurate due to different range of initial drug concentration, it is clear that enhanced 5-FU adsorption was reported for nanogel, NiO/geopolymer and metal organic framework adsorbents with capacities of 659.7 mg/g, 329.7 mg/g and 645.4 mg/g respectively. On the other hand, materials designed for drug delivery purposes including chitosan-functionalized graphene oxide, chitosan modified single-walled carbon nanotube and mesoporous silica displayed an adsorption capacity of 44.29 mg/g, 31.77 mg/g and 55 mg/g respectively which are closer to the adsorption capacities obtained for

Table 7
Isotherm model parameters for GO/HAp-8 composite (pH: 2.0, adsorbent dosage: 0.05 g).

Isotherm Model	Parameter	Value
Langmuir	q_m (mg/g)	47.3
	k_L (L/mg)	0.00146
	R^2	0.9522
	R_L	0.5330
	RMSE (mg/g)	2.658
	AIC	14.732
Freundlich	n	1.8936
	k_F (mg/(g(mg/L)$^{1/n}$))	0.7279
	R^2	0.9616
	RMSE (mg/g)	1.936
	AIC	10.927
Dubinin-Radushkevich	q_D (mg/g)	27.03
	k_D (mol^2/J^2)	0.0058
	E (kJ/mol)	9.28
	R^2	0.8596
	RMSE (mg/g)	6.042
	AIC	24.585

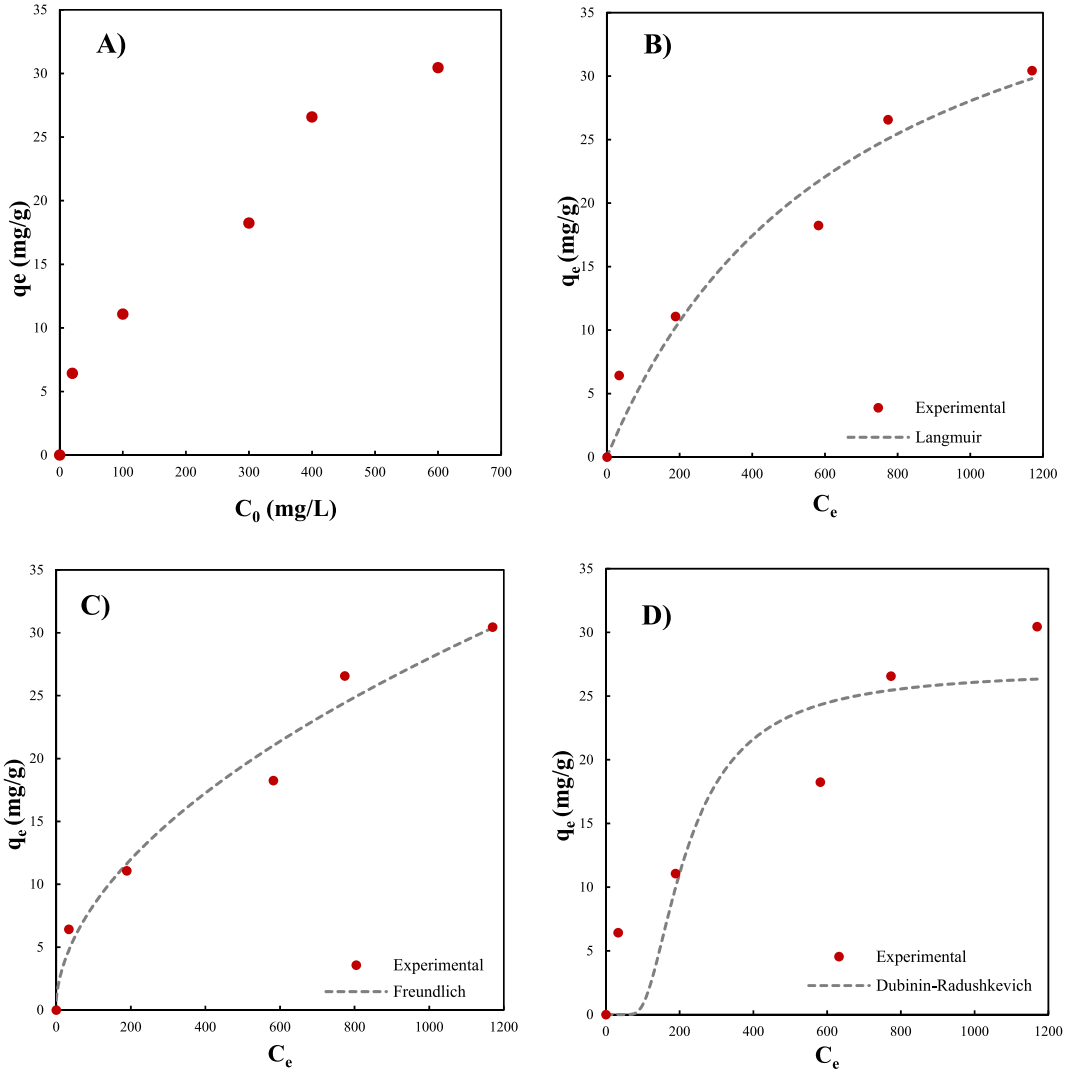

Fig. 9. A) Adsorption values against initial concentration of drug. Nonlinear fitting of adsorption isotherm models for GO/HAp-8 composite: B) Langmuir model, C) Freundlich model, D) Dubinin-Radushkevich model (pH: 2.0, adsorbent dosage: 0.05 g).

this study.

3.11. Drug release studies

3.11.1. Drug release kinetics of GO/HAp composite

Drug release kinetic models were originated under the optimum conditions determined from experimental design for the adsorption of 5-FU onto GO/HAp (GO: % 8, initial drug concentration: 0.02 mg/ml, pH: 2). The effect of release medium pH value, GO ratio and initial drug concentration were investigated to gain a better insight on the release behavior.

Three distinct pH values including pH 1.2, 5.0 and 7.4 were selected as the release medium pH, representing the pH value of stomach, cancerous and physiological medium respectively. Release kinetics were evaluated against five different kinetic models including zero-order, first-order, Higuchi, Korsmeyer-Peppas and Hixson-Crowell model. Obtained data from the drug release studies were both fitted to linear (Fig. S3–5) and nonlinear versions (Fig. S11–13) of the model equations apart from zero-order and calculated parameters were detailed in Table 10. As observed from the linear fitting parameters in Table 10, Higuchi model was emerged as the best fitting model displaying R^2 values of 0.9707 and 0.9899 for pH 1.2 and 5.0 conditions respectively, together with the lowest RMSE and AIC values. Under these conditions, drug release was understood to occur through diffusion and dissolution being directly proportional to square root of time [92]. While in the case of pH 7.4, compatibility with zero order model was observed with a R^2 value of 0.9492, indicating a controlled release of drug with a near constant release rate. In drug release systems with zero order release kinetics, sudden release could be prevented by ensuring the release of the drug at a constant rate and the concentration of the drug can be

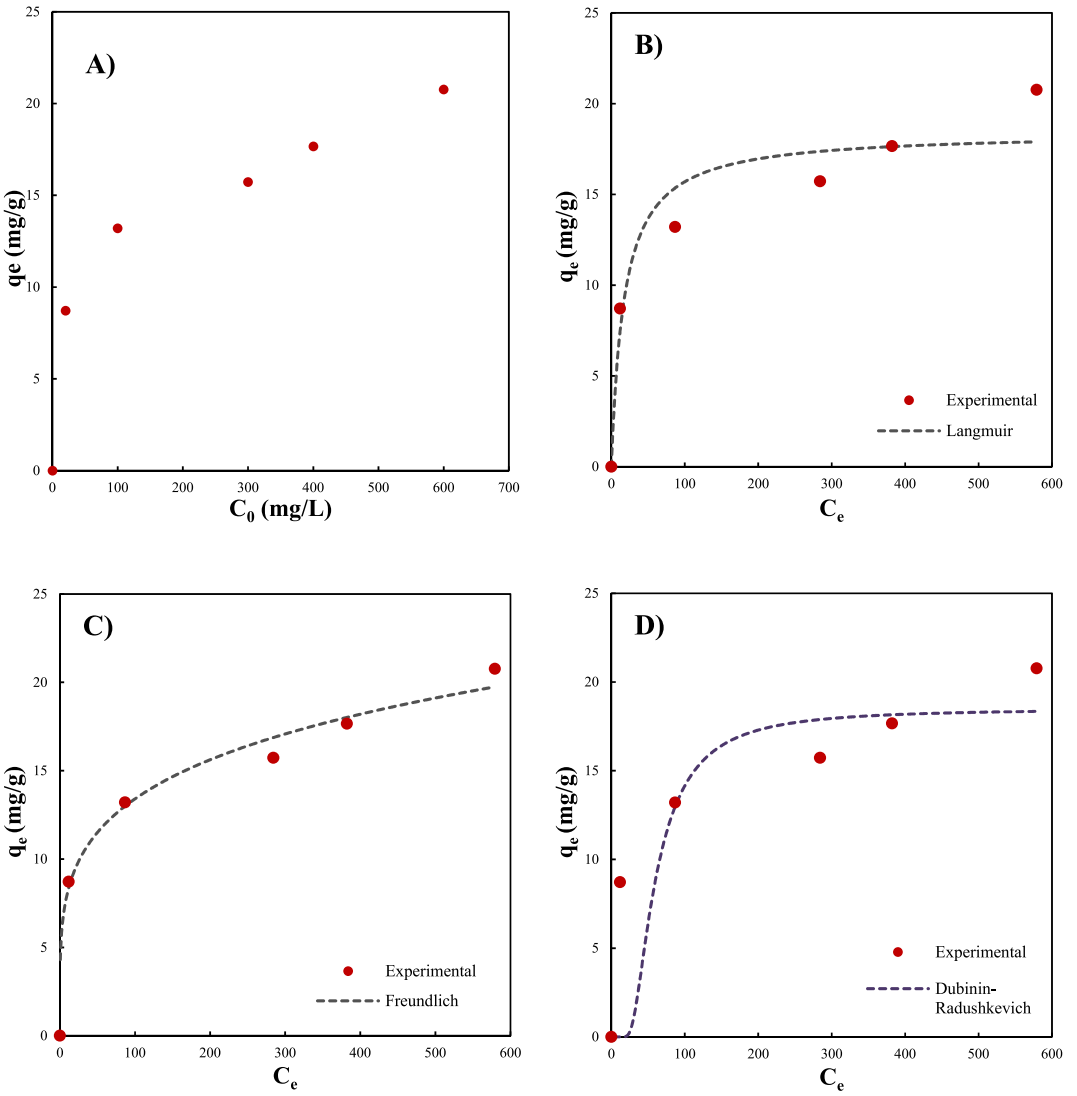

Fig. 10. A) Adsorption values against initial concentration of drug. Nonlinear fitting of adsorption isotherm models for GO-NH_2/HAp-8 composite: B) Langmuir model, C) Freundlich model, D) Dubinin-Radushkevich model (pH: 2.0, adsorbent dosage: 0.05 g).

maintained within the therapeutic window limits for longer periods. Providing this release profile allows limiting side effects due to immediate release and reducing dosing frequency. In certain drug delivery applications, zero order drug release kinetic could be targeted for the drugs with short biological half-life and narrow therapeutic window including 5-FU [93]. In that context, release profile of 5-FU from GO/HAp at physiological pH could be interpreted as a desired profile in such cases.

On the other hand, evaluation by nonlinear fitting of the drug release data resulted in compliance to Korsmeyer-Peppas model for all pH conditions, displaying slightly higher R^2 values compared to Higuchi model. The R^2 values were obtained as 0.9847, 0.9928 and 0.9694 for pH 1.2, 5.0 and 7.4 conditions respectively. The fact that the drug release exponent (n) < 0.5 indicates a Fickian type diffusion, which is the case for pH 1.2 ($n = 0.408$) and 5.0 ($n = 0.4547$) conditions, could be interpreted as the release of 5-FU in lower pH mediums influenced by Fickian Diffusion [94]. Whereas, n value for pH 7.4 ($n = 0.7449$) condition is in the range of 0.5 and 1, denoting that the release system in physiological pH follows anomalous or non-Fickian diffusion and different mechanisms might have affected the release along with diffusion [95].

The initial release ratios at the end of first hour were obtained as 49.9 %, 43.5 % and 24.7 % for pH 1.2, 5.0 and 7.4 respectively (Fig. 11A). The relative increase in burst release with pH decrease is a sign of pH sensitive release of 5-FU from GO/HAp, a behavior which was also reported in several studies on HAp based drug carriers [96–98]. It is known that solubility of HAp increases at low pH values leading to release of Ca^{2+} and PO_4^{-3} from the surface. The higher release rate at pH 1.2 can be attributed to the diffusion of drug molecules close to the surface and the acceleration of these drug molecules' diffusion due to the release of more Ca^{+2} and PO_4^{-3} ions under these conditions. Higher release rates at lower pH values is a favorable aspect for the 5-FU delivery around tumor cells and inflammatory tissues, as it is known that lower pH values are observed in these regions [99]. Hence, aforementioned zero order release

Table 8
Isotherm model parameters for GO-NH_2/HAp-8 composite (pH: 2.0, adsorbent dosage: 0.05 g).

Isotherm Model	Parameter	Value
Langmuir	q_m (mg/g)	18.4
	k_L (L/mg)	0.0574
	R^2	0.9381
	R_L	0.0282
	RMSE (mg/g)	2.238
	AIC	12.665
Freundlich	n	4.5364
	k_F (mg/(g(mg/L)$^{1/n}$))	4.8580
	R^2	0.9682
	RMSE (mg/g)	0.691
	AIC	−1.443
Dubinin-Radushkevich	q_D (mg/g)	18.49
	k_D (mol^2/J^2)	0.00044
	E (kJ/mol)	33.71
	R^2	0.6859
	RMSE (mg/g)	3.388
	AIC	17.643

Table 9
Comparison of 5-FU adsorption capacities among relevant literature studies.

Adsorbent	Adsorption capacity	Initial drug concentration	Refs.
Chitosan-functionalized graphene oxide	44.29 mg/g	0–80 mg/L (20 °C)	[41]
Chitosan modified single-walled carbon nanotube	31.77 mg/g	0–100 mg/L (25 °C)	[42]
Cellulose nanofibrils	0.123 mg/g	2–10 mg/L	[45]
Mesoporous silica SBA-15	55 mg/g	0-5x10^{-2} mol/L	[43]
β-cyclodextrin grafted poly(N-vinylcaprolactam) nanogel	659.7 mg/g	0–1000 mg/L	[88]
Mesoporous silica (MCM-48)/biopolymer	141.2–191 mg/g	0–900 mg/L	[89]
Poly(vinyldiaminotriazine) nanoparticle	6.897 mg/g	0–0.025 mg/ml	[90]
NiO/geopolymer	329.7 mg/g	0–250 mg/L (40 °C)	[91]
Graphene oxide/gelatin	108.7 mg/g	0–8 mg/ml	[47]
MIL-101-NH2 (Co/Fe) bi-metal–organic framework	645.4 mg/g	0–500 mg/L	[46]
Alginate/geoplymer hybrid beads	6.28 mg/g	0.1–40 mg/L	[44]
Graphene oxide/hydroxyapatite	47.3 mg/g	0–600 mg/L	This study.
Amine modified graphene oxide/hydroxyapatite	18.4 mg/g	0–600 mg/L	This study.

Table 10
Kinetic model parameters derived from linear and nonlinear fitting of % drug release from GO/HAp-8 composite at various pH values (temperature: 37 °C).

Model		Linear Fitting			Nonlinear Fitting		
		pH			pH		
		1.2	5.0	7.4	1.2	5.0	7.4
Zero Order	**k_0 (h^{-1})**	11.009	10.951	13.203	-	-	-
	R^2	0.8568	0.9026	**0.9492**	**-**	**-**	**-**
	RMSE	12.134	9.694	8.237	-	-	-
	AIC	52.419	47.930	44.672	-	-	-
First Order	**k_1** (h^{-1})	0.4537	0.3392	0.4376	0.4434	0.3619	0.2916
	R^2	0.9201	0.9609	0.8981	0.9570	0.9590	0.9462
	RMSE	7.274	5.587	8.990	6.649	6.295	8.471
	AIC	42.187	36.909	46.422	40.389	39.295	45.234
Korsmeyer-Peppas	**n** (h^{-1})	0.4702	0.4856	1.3652	0.408	0.4547	0.7449
	R^2	0.9608	0.9806	0.8927	**0.9847**	**0.9928**	**0.9694**
	RMSE	5.108	3.081	23.031	3.961	2.633	6.390
	AIC	31.928	22.827	59.034	30.031	21.861	39.596
Higuchi	**k_H** ($h^{-1/2}$)	37.715	35.652	33.903	37.715	35.652	33.903
	R^2	**0.9707**	**0.9899**	0.9246	0.9707	0.9899	0.9246
	RMSE	5.489	3.125	10.031	5.489	3.125	10.031
	AIC	36.555	25.290	48.615	36.555	25.290	48.615
Hixson-Crowell	**k_{HC}** (h^{-1})	0.4797	0.4487	0.509	0.5247	0.4340	0.3687
	R^2	0.9414	0.8895	0.9320	0.9294	0.9373	0.9678
	RMSE	7.246	7.548	10.863	8.516	7.780	6.551
	AIC	42.109	42.925	50.207	45.339	43.532	40.092

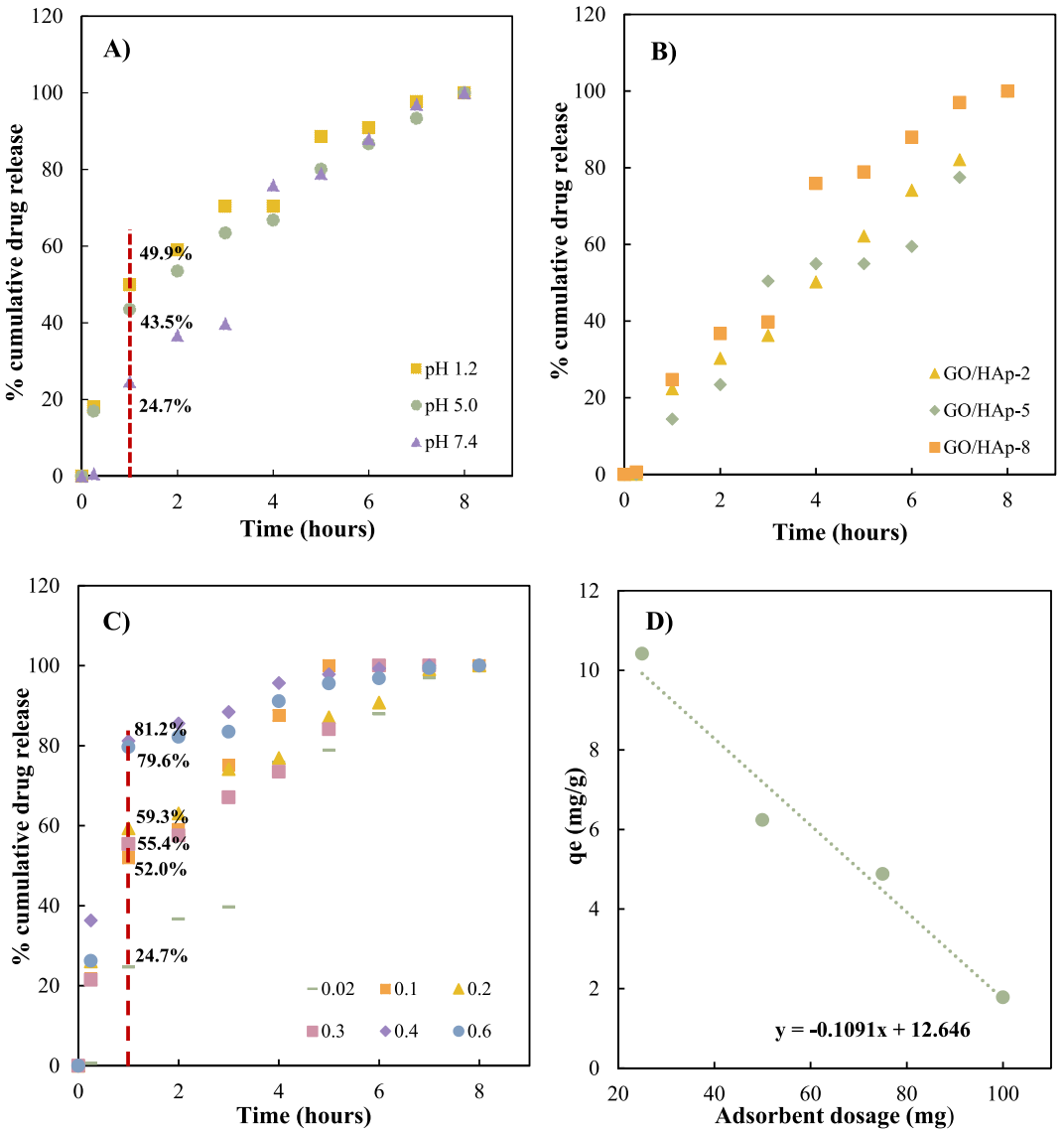

Fig. 11. Release profiles of 5-FU from A) GO/HAp-8 at pH 1.2, 5.0 and 7.4 (temperature: 37 °C), B) GO/HAp-2, GO/HAp-5 and GO/HAp-8 at pH 7.4 (temperature: 37 °C), C) GO/HAp-8 loaded with various 5-FU content, D) Various GO/HAp-8 amounts in proportion to total adsorbed drug.

and pH sensitive behavior under in vitro conditions confirmed the suitability of GO/HAP as a carrier for 5-FU.

The release profiles of all produced GO/HAp composites were evaluated at physiological pH in order to observe the possible effect of GO ratio and a significant change in initial burst value was not determined within samples (Fig. 11B). Linear fitting of the release data (Fig. S6 and Fig. S7) displayed better compliance with zero order model at lower GO ratios, R^2 values of 0.9868 (GO/HAp-2) and 0.9509 (GO/HAp-5) respectively (Table 11). Similar to the case in GO/HAp-8, compliance of GO/HAp-2 ($R^2 = 0.9884$) and GO/HAp-5 ($R^2 = 0.9546$) release data shifted to Korsmeyer-Peppas model as the best fit for nonlinear fitting.

The effect of initial drug concentration in adsorption medium on burst release and release profile was investigated as presented in Fig. 11C. Similar to previous reports in literature, increasing drug loadings resulted in higher burst release ratios, which could be attributed to presence of more drug molecules attached to composite surface [93]. The R^2 values of zero order model lessened with higher drug contents, indicating a diversion from constant rate release (Table 12). For GO/HAp-8 composite, influence of adsorbent dosage was also examined at various adsorbent dosage values as presented in Fig. 11D. Similar to several literature studies, adsorption capacity displayed a decreasing trend, possibly related to the agglomeration of GO/HAp particles leading to less available active adsorption sites for 5-FU molecules [100–102].

3.11.2. Drug release kinetics of GO-NH_2/HAp composite

The drug release profiles GO-NH_2/HAp composite in comparison with GO/HAp with changing pH were presented in Fig. 12. Drug

Table 11
Kinetic model parameters derived from linear and nonlinear fitting of % drug release from GO/HAp-2, GO/HAp-5 and GO/HAp-8 composites (pH 7.4, temperature: 37 °C).

Model		Linear Fitting			Nonlinear Fitting		
		GO/HAp-2	GO/HAp-5	GO/HAp-8	GO/HAp-2	GO/HAp-5	GO/HAp-8
Zero Order	**k_0 (h^{-1})**	11.896	11.409	13.203	-	-	-
	R^2	**0.9868**	**0.9509**	**0.9492**	**-**	**-**	**-**
	RMSE	3.709	6.987	8.237	-	-	–
	AIC	28.717	41.382	44.672	-	-	-
First Order	**k_1 (h^{-1})**	0.2315	0.1902	0.4376	0.2115	0.1972	0.2916
	R^2	0.9611	0.9331	0.8981	0.9430	0.9252	0.9462
	RMSE	7.793	8.650	8.990	7.709	8.628	8.471
	AIC	43.564	45.651	46.422	43.348	45.599	45.234
Korsmeyer-Peppas	**n (h^{-1})**	0.7320	0.8760	1.3652	0.8939	0.8761	0.7449
	R^2	0.9613	0.9454	0.8927	**0.9884**	**0.9546**	**0.9694**
	RMSE	5.337	7.083	21.849	3.483	6.719	6.390
	AIC	32.714	37.809	59.034	27.458	40.599	39.596
Higuchi	**k_H ($h^{-1/2}$)**	28.932	27.619	33.903	28.932	27.619	33.903
	R^2	0.9046	0.8765	0.9246	0.9046	0.8765	0.9246
	RMSE	9.973	11.082	10.031	9.973	11.082	10.031
	AIC	48.497	50.606	48.615	48.497	50.606	48.615
Hixson-Crowell	**k_{HC} (h^{-1})**	0.4252	0.4019	0.509	0.2767	0.2593	0.3687
	R^2	0.7753	0.7106	0.9320	0.9641	0.9396	0.9678
	RMSE	13.730	14.168	10.863	6.114	7.751	6.551
	AIC	54.892	55.520	50.207	38.712	43.456	40.092

Table 12
Zero Order kinetic model parameters of GO/HAp-8 composite for different initial drug concentrations (pH: 7.4, temperature: 37 °C).

Model	Zero Order			
Initial drug concentration (mg/ml)	**k_0 (h^{-1})**	**R^2**	**RMSE**	**AIC**
0.02	13.203	0.9492	8.237	44.672
0.1	11.427	0.8173	14.564	56.072
0.2	10.233	0.8035	13.639	54.759
0.3	12.389	0.8682	11.535	46.589
0.4	8.9629	0.5767	20.697	63.099
0.6	9.4293	0.6138	20.160	62.574

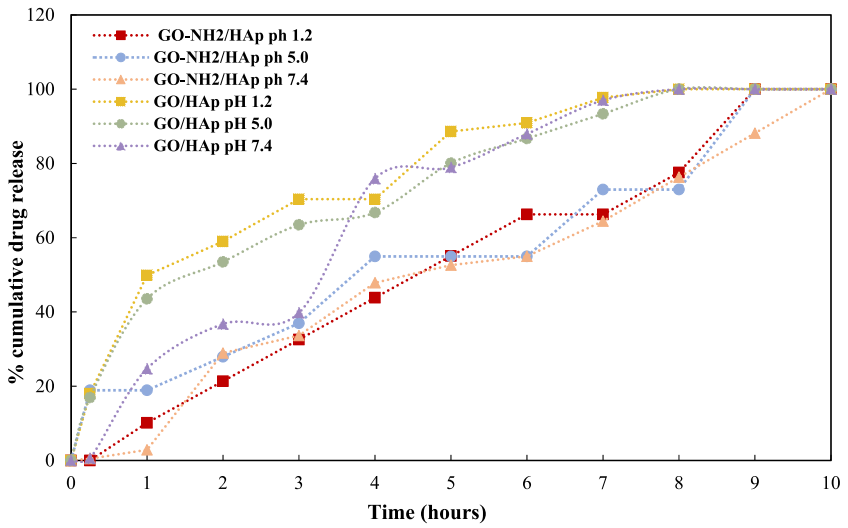

Fig. 12. Release profiles of GO-NH_2/HAp-8 in comparison with GO/HAp-8 at pH 1.2, 5.0 and 7.4 (temperature: 37 °C) in proportion to total adsorbed drug.

release was completed after approximately 10 h at all pH values and compared to GO/HAp-8, the initial burst release occurred at lower levels. At the end of first hour, 10.1 %, 18.9 % and 2.8 % of the total drug were released at pH 1.2, 5.0 and 7.4 respectively. Based on the linear fitting of release profiles obtained for different kinetic models (Fig. S8–10), calculations revealed that 5-FU release from GO-NH_2/HAp followed zero order release kinetic at all pH values, similar to GO/HAp at physiological pH (Table 13). However, nonlinear fitting resulted in slightly higher R^2 values for pH 1.2 ($R^2 = 0.9886$) and 7.4 ($R^2 = 0.9801$) for Korsmeyer-Peppas compared to zero order model (Fig. S16–18). Atall three pH conditions, n values were obtained in the range of 0.5 and 1, indicating a disordered transport state (non-Fickian). Overall data demonstrated that amine modification of GO not only improved the 5-FU adsorption but also resulted in a more controlled release profile.

The effect of amine modification on controlled release of drugs such as ibuprofen and paracetamol have been investigated and reported in literature. For ibuprofen drug, amine modified mesoporous magnesium carbonate (MMC) was studied as a carrier and displayed a more retarded release of drug in comparison with unmodified MMC. Increasing the amount of amine groups reduced the initial burst release ratio which was explained by the strong interactions between carboxyl group of ibuprofen and amine groups of modified MMC [103]. Another study examined the mesoporous silica KCC-1(KCC-1) in comparison with its amine functionalized version (KCC-1-NH_2) as a drug carrier of paracetamol. In vitro release studies evidently showed that KCC-1-NH_2 sample provided slower release rate than unmodified KCC-1. This effect was related to stronger interactions between amine groups of KCC-1-NH_2 and amide (–CO–NH2) and hydroxyl (–OH) groups of paracetamol. Also, reduced PBS entrance in the pores by NH_2 groups and steric hindrance of NH_2 groups were stated as the reasons of slower initial drug release [104]. Accordingly, the more controlled release from GO-NH_2/HAp could be attributed to the interactions between H atoms of 5-FU and amine groups of GO-NH_2/HAp, possibly stronger than the electrostatic interactions and π-π interaction occurred with GO/HAp composite. Literature studies conducted with hydroxyapatite/graphene oxide content for the controlled release of various drugs are summarized in Table 14.

4. Conclusions

The present study focused on the production of graphene oxide/hydroxyapatite and amine functionalized graphene oxide/hydroxyapatite composites as drug carriers for 5-FU, optimization of 5-FU adsorption via experimental design studies and investigation of 5-FU release kinetics. The morphological and chemical structure of GO/HAp and GO-NH_2/HAp composites were investigated by FTIR, TGA and SEM analysis measurements, confirming the achieved composite formation. Experimental design studies pointed out the enhanced adsorption percentages of 5-FU at increasing GO content, low adsorption medium pH value and low initial drug concentration. Further adsorption studies with GO-NH_2/HAp composites demonstrated that amine modification had a distinct positive influence on adsorption of 5-FU, allowing the adsorption percentage of 40.9 % at pH 2. Adsorption isotherm studies revealed the compatibility of composites with Freundlich model before and after amine modification. From in vitro release studies, it was observed that GO/HAp composites followed Higuchi and Korsmeyer-Peppas kinetic models depending on release medium pH value, whereas GO-NH_2/HAp composites followed zero order and Korsmeyer-Peppas kinetic models at all pH conditions indicating amine modification's positive effect on prolonged release of 5-FU. Overall results suggested that both GO/HAp and GO-NH_2/HAp composites had a potential for the adsorption and delivery of 5-FU drug in clinical applications.

Table 13
Kinetic model parameters derived from linear and nonlinear fitting of % drug release from GO-NH_2/HAp-8 composite (pH: 7.4, temperature: 37 °C).

Model		Linear Fitting			Nonlinear Fitting		
		1.2	5.0	7.4	1.2	5.0	7.4
Zero Order	**k_0 (h^{-1})**	10.291	9.0641	9.7005	-	-	-
	R^2	**0.9880**	**0.9583**	**0.9779**	**-**	**-**	**-**
	RMSE	3.744	6.240	4.810	-	-	-
	AIC	34.082	46.344	40.097	-	-	-
First Order	**k_1 (h^{-1})**	0.1815	0.1561	0.2004	0.1790	0.1887	0.1675
	R^2	0.9790	0.9462	0.9095	0.9292	0.9059	0.9381
	RMSE	8.724	10.013	8.331	9.091	9.372	8.055
	AIC	54.386	57.692	53.279	55.374	56.105	52.472
Korsmeyer-Peppas	**n (h^{-1})**	1.1997	0.4980	1.4497	0.9562	0.7569	0.9144
	R^2	0.9794	0.8637	0.9464	**0.9886**	0.9515	**0.9801**
	RMSE	8.197	10.365	14.818	3.645	6.729	4.566
	AIC	48.726	53.890	61.753	33.442	48.153	38.850
Higuchi	**k_H ($h^{-1/2}$)**	26.801	27.420	25.653	26.801	27.420	25.653
	R^2	0.8798	0.9080	0.8849	0.8798	0.9080	0.8849
	RMSE	11.847	9.267	10.981	11.847	9.267	10.981
	AIC	61.730	55.836	59.908	61.730	55.836	59.908
Hixson-Crowell	**k_{HC} (h^{-1})**	0.4165	0.3930	0.3335	0.2341	0.2425	0.2197
	R^2	0.7876	0.7476	0.7773	0.9566	0.9243	0.9586
	RMSE	18.146	18.076	12.727	7.117	8.408	6.587
	AIC	71.963	71.870	63.449	49.500	53.501	47.641

Table 14
Examples of literature studies including graphene oxide/hydroxyapatite composite for drug delivery applications.

Material	Drug	Release percentage	Refs.
Graphene oxide/hydroxyapatite	Ibuprofen	94 % (48 h)	[19]
Mesoporous hydroxyapatite/graphene oxide in the presence of chitosan	Naproxen	43.8–68 % (14 days)	[68]
Graphene oxide/hydroxyapatite	Amoxicillin	40–60 % (96 h)	[31]
Hydroxyapatite nanorod/graphene oxide	Protein	32–91 % (50 h)	[97]
Hydroxyapatite nanorod/graphene oxide	Doxorubicin	20–70 % (60 min)	[33]
Surface modified hydroxyapatite/graphene oxide	Aspirin	30–65 % (70 h)	[105]
Gelatin/hydroxyapatite/graphene oxide	Vitamin D	24–96 % (384 h)	[32]
Strontium substituted hydroxyapatite/graphene oxide	Curcumin	50–75 % (168 h)	[106]
Graphene oxide/hydroxyapatite	5-Fluorouracil	19–32 % (10 h)	This study.
Amine modified graphene oxide/hydroxyapatite	5-Fluorouracil	14–40 % (10 h)	This study.

Data availability

Data will be made available on request.

CRediT authorship contribution statement

Ebru Kahraman: Writing – original draft, Software, Methodology, Investigation, Conceptualization. **Gulhayat Nasun-Saygili:** Writing – review & editing, Supervision, Resources, Methodology.

Declaration of competing interest

The authors declare that they have no known competing financial interests or personal relationships that could have appeared to influence the work reported in this paper.

Acknowledgements

This study was supported by Istanbul Technical University BAP (42197).

Appendix A. Supplementary data

Supplementary data to this article can be found online at https://doi.org/10.1016/j.heliyon.2024.e38494.

References

[1] H. Ding, J. Yong, J. Zhang, B. Chen, B. Ding, X. Wang, Anchoring Pd nanoparticles on hollow CuS nanoparticles for enhanced NIR induced photothermal effects for chemotherapeutic drug delivery and gastric cancer treatment, Ceram. Int. 48 (11) (2022) 16085–16090.
[2] G. Liu, L. Yang, G. Chen, F. Xu, F. Yang, H. Yu, L. Li, X. Dong, J. Han, C. Cao, J. Qi, J. Su, X. Xu, X. Li, B. Li, A review on drug delivery system for tumor therapy, Front. Pharmacol. 12 (2021) 735446.
[3] J. Di, X. Gao, Y. Du, H. Zhang, J. Gao, A. Zheng, Size, shape, charge and "stealthy" surface: carrier properties affect the drug circulation time in vivo, Asian J. Pharm. Sci. 16 (4) (2021) 444–458.
[4] J. Siepmann, R.A. Siegel, M.J. Rathbone, The need for drugs and drug delivery systems, fundamentals and applications of controlled release, Drug Deliv. (2012) 3–18.
[5] M.F.H. Abd El-Kader, M.K. Ahmed, M.T. Elabbasy, M. Afifi, A.A. Menazea, Morphological, ultrasonic mechanical and biological properties of hydroxyapatite layers deposited by pulsed laser deposition on alumina substrates, Surf. Coat. Technol. 409 (2021) 126861.
[6] X. Jiang, X. Liu, J. Cai, S. Wei, Y. Wang, Z. Duan, Z. Zhou, R. Sun, X. Qu, Y. Tang, Fabrication and properties of multi-functional polydopamine coated Cu/F-codoped hydroxyapatite hollow microspheres as drug carriers, Colloids Surf. B Biointerfaces 222 (2023) 113097.
[7] M. Du, J. Chen, K. Liu, H. Xing, C. Song, Recent advances in biomedical engineering of nano-hydroxyapatite including dentistry, cancer treatment and bone repair, Compos. B Eng. 215 (2021) 108790.
[8] M. Xiaoyu, D. Xiuling, Z. Chunyu, S. Yi, Q. Jiangcha, Y. Yuan, L. Changsheng, Polyglutamic acid-coordinated assembly of hydroxyapatite nanoparticles for synergistic tumor-specific therapy, Nanoscale 32 (11) (2019) 15312–15325.
[9] B. Palazzo, M.C. Sidoti, N. Roveri, A. Tampieri, M. Sandri, L. Bertolazzi, F. Galbusera, G. Dubini, P. Vena, R. Contro, Controlled drug delivery from porous hydroxyapatite grafts: an experimental and theoretical approach, Mater. Sci. Eng. C. 25 (2) (2005) 207–213.
[10] D. Loca, J. Locs, A. Dubnika, V. Zalite, L. Berzina-Cimdina, 9 - porous hydroxyapatite for drug delivery, hydroxyapatite (Hap) for biomedical applications, Hydroxyapatite (Hap) for Biomedical Applications (2015) 189–209.
[11] G. Devanand Venkatasubbu, S. Ramasamy, G.S. Avadhani, V. Ramakrishnan, J. Kumar, Surface modification and paclitaxel drug delivery of folic acid modified polyethylene glycol functionalized hydroxyapatite nanoparticles, Powder Technol. 235 (2013) 437–442.
[12] J. Prakash, T. Sushil Kumar, K.S. Venkataprasanna, R. Niranjan, M. Kaushik, D.B. Samal, G. Devanand Venkatasubbu, PVA/alginate/hydroxyapatite films for controlled release of amoxicillin for the treatment of periodontal defects, Appl. Surf. Sci. 495 (2019) 143543.
[13] J. He, X. Hu, J. Cao, Y. Zhang, J. Xiao, l. Peng, D. Chen, C. Xiong, L. Zhang, Chitosan-coated hydroxyapatite and drug-loaded polytrimethylene carbonate/polylactic acid scaffold for enhancing bone regeneration, Carbohydr. Polym. 253 (2021) 117198.

[14] J. Liu, S. Lin, J. Dang, S. Wang, W. Cheng, Z. Ran, H. Zhu, H. Deng, C. Xiong, W. Xu, Z. Huang, P. Xu, H. Xu, Anticancer and bone-enhanced nano-hydroxyapatite/gelatin/polylactic acid fibrous membrane with dual drug delivery and sequential release for osteosarcoma, Int. J. Biol. Macromol. 240 (2023) 124406.
[15] S.C. Veerla, D.R. Kim, J. Kim, H. Sohn, S.Y. Yang, Controlled nanoparticle synthesis of Ag/Fe co-doped hydroxyapatite system for cancer cell treatment, Mater. Sci. Eng. C. 98 (2019) 311–323.
[16] H. Kim, S. Mondal, S. Bharathiraja, P. Manivasagan, M.S. Moorthy, J. Oh, Optimized Zn-doped hydroxyapatite/doxorubicin bioceramics system for efficient drug delivery and tissue engineering application, Ceram. Int. 44 (6) (2018) 6062–6071.
[17] H. Li, X. Sun, Y. Li, B. Li, C. Liang, H. Wang, Preparation and properties of carbon nanotube (Fe)/hydroxyapatite composite as magnetic targeted drug delivery carrier, Mater. Sci. Eng. C. 97 (2019) 222–229.
[18] V. Zeyni, S. Karimi, H. Namazi, Surface PEGylation of ZIF-8 metal-organic framework based on magnetic hydroxyapatite as a pH/magnetic targeting responsive system for anticancer drug delivery, Micropor. Mesopor. Mat. 354 (2023) 112544.
[19] C. Yao, J. Zhu, A. Xie, Y. Shen, H. Li, B. Zheng, Y. Wei, Graphene oxide and creatine phosphate disodium dual template-directed synthesis of GO/hydroxyapatite and its application in drug delivery, Mater. Sci. Eng. C. Mater. Biol. Appl. 73 (2017) 709–715.
[20] Y. Zhao, Y. Qiu, Z. Fang, F. Pu, R. Sun, K. Chen, Y. Tang, Preparation and characterization of Sr-substituted hydroxyapatite/reduced graphene oxide 3D scaffold as drug carrier for alendronate sodium delivery, Ceram. Int. 48 (24) (2022) 36601–36608.
[21] S. Yu, X. Wang, L. Lv, T. Liu, Q. Guan, Borneol-modified PEGylated graphene oxide as a nanocarrier forbrain-targeted delivery of ginsenoside Rg1 against depression, Int. J. Pharm. 643 (2023) 123284.
[22] T.K. Ghorai, Graphene oxide-based nanocomposites and biomedical applications, Funct. Polysaccharides Biomed. Appl. (2019) 305–328.
[23] E.L.K. Chng, M. Pumera, The toxicity of graphene oxides: dependence on the oxidative methods used, Chem. Eur J. 19 (25) (2013) 8227–8235.
[24] Ü.H. Erol, E. Güncüm, N. Işıklan, Development of chitosan-graphene oxide blend nanoparticles for controlled flurbiprofen delivery, Int. J. Biol. Macromol. 246 (2023) 125627.
[25] A. Deb, V. Raghavan, Camptothecin loaded graphene oxide nanoparticle functionalized with polyethylene glycol and folic acid for anticancer drug delivery, J. Drug Deliv. Sci. Technol. 43 (2018) 333–342.
[26] M. Hasanin, N.F. Taha, A.R. Abdou, L.H. Emara, Green decoration of graphene oxide Nano sheets with gelatin and gum Arabic for targeted delivery of doxorubicin, Biotechnol. Rep. 34 (2022) e00722.
[27] Z. Rao, H. Ge, L. Liu, C. Zhu, L. Min, M. Liu, L. Fan, D. Li, Carboxymethyl cellulose modified graphene oxide as pH-sensitive drug delivery system, Int. J. Biol. Macromol. 107 (2018) 1184–1192.
[28] G. Schifino, C. Gasparini, S. Drudi, M. Giannelli, G. Sotgiu, T. Posati, R. Zamboni, E. Treossi, E. Maccaferri, L. Giorgini, R. Mazzaro, V. Morandi, V. Palermo, M. Bertoldo, A. Aluigi, Keratin/Polylactic acid/graphene oxide composite nanofibers for drug delivery, Int. J. Pharm. 623 (2022) 121888.
[29] M. Pooresmaeil, H. Namazi, β-Cyclodextrin grafted magnetic graphene oxide applicable as cancer drug delivery agent: synthesis and characterization, Mater. Chem. Phys. 218 (2018) 62–69.
[30] S. Javanbakht, M. Pooresmaeil, H. Namazi, Green one-pot synthesis of carboxymethylcellulose/Zn-based metal-organic framework/graphene oxide bio-nanocomposite as a nanocarrier for drug delivery system, Carbohydr. Polym. 208 (2019) 294–301.
[31] O.K. Taghzouti, K.E. Mabrouk, M. Bricha, K. Nouneh, Controlled adsorption and release of amoxicillin in GO/HA composite materials, SN Appl. Sci. 1 (2019) 226.
[32] R. Mahdavi, G. Belgheisi, M. Haghbin-Nazarpak, M. Omidi, A. Khojasteh, M. Solati-Hashjin, Bone tissue engineering gelatin-hydroxyapatite/graphene oxide scaffolds with the ability to release vitamin D: fabrication, characterization, and in vitro study, J. Mater. Sci. Mater. Med. 31 (11) 97.
[33] R. Sang, M. Chen, Y. Yang, Y. Li, J. Shi, Y. Deng, X. Chen, W. Yang, HAp@GO drug delivery vehicle with dual-stimuli-triggered drug release property and efficient synergistic therapy function against cancer, J. Biomed. Mater. Res. A. 107 (10) 2296-2309.
[34] D. Ulker, I. Barut, E. Şener, V. Bütün, Advanced liposome based PEGylated microgel as a novel release system for 5-fluorouracil against MCF-7 cancer cell, Eur. Polym. J. 146 (2021) 110270.
[35] J. Hu, A. Li, Y. Guo, T. Ma, S. Feng, The relationship between tumor metabolism and 5-fluorouracil resistance, Biochem. Pharmacol. 218 (2023) 115902.
[36] D. Radha, J.S. Lal, K.S. Devaky, Release studies of the anticancer drug 5-fluorouracil from chitosan-banana peel extract films, Int. J. Biol. Macromol. 256 (2024) 128460.
[37] P. Kishi, C.J. Price, Life-threatening reaction with topical 5-Fluorouracil, Drug, Saf. Case. Rep. 5 (2018) 4.
[38] Y. Lin, Y. Li, C.P. Ooi, 5-Fluorouracil encapsulated HA/PLGA composite microspheres for cancer therapy, J. Mater. Sci. Mater. Med. 23 (10) (2012) 2453–2460.
[39] T. Basargan, N. Erdol-Aydin, G. Nasun-Saygili, Hydroxyapatite-chitosan biocomposites synthesized in the simulated body fluid and their drug loading studies, J. Mater. Sci. Mater. Med. 28 (11) (2017) 180.
[40] B. Zhang, Y. Yan, Q. Shen, D. Ma, L. Huang, X. Cai, S. Tan, A colon targeted drug delivery system based on alginate modificated graphene oxide for colorectal liver metastasis, Mater. Sci. Eng. C. 79 (2017) 185–190.
[41] P. Miralinaghi, P. Kashani, E. Moniri, M. Miralinaghi, Non-linear kinetic, equilibrium, and thermodynamic studies of 5-fluorouracil adsorption onto chitosan–functionalized graphene oxide, Mater. Res. Express 6 (6) (2019) 065305.
[42] S. Karimidost, E. Moniri, M. Miralinaghi, Thermodynamic and kinetic studies sorption of 5-fluorouracil onto single walled carbon nanotubes modified by chitosan, Kor, J. Chem. Eng. 36 (2019) 1115–1123.
[43] E. Beňová, D. Bergé-Lefranc, V. Zeleňák, M. Almáši, V. Huntošová, V. Hornebecq, Adsorption properties, the pH-sensitive release of 5-fluorouracil and cytotoxicity studies of mesoporous silica drug delivery matrix, Appl. Surf. Sci. 504 (2020) 144028.
[44] A.B. Amor, M. Arenas, J. Martín, A. Ouakouak, J.L. Santos, I. Aparicio, E. Alonso, N. Hamdi, Alginate/geopolymer hybrid beads as an innovative adsorbent applied to the removal of 5-fluorouracil from contaminated environmental water, Chemosphere 335 (2023) 139092.
[45] M.S. Sajab, D. Mohan, J. Santanaraj, C.H. Chia, H. Kaco, S. Harun, N.H.N. Kamarudin, Telescopic synthesis of cellulose nanofibrils with a stable dispersion of Fe(0) nanoparticles for synergistic removal of 5-fluorouracil, Sci. Rep. 9 (2019) 11703.
[46] L.R. Rad, H. Faramarzi, M. Anbia, M. Irani, Adsorption of doxorubicin and 5-Fluorouracil anticancer drugs from aqueous media using MIL-101-NH_2 (Co/Fe) bi-metal–organic framework, Sep. Purif. Technol. 339 (2024) 126597.
[47] E. Kahraman, N.E. Aydin, G. Nasun-Saygili, Optimization of 5-FU adsorption on gelatin incorporated graphene oxide nanocarrier and application for antitumor activity, J. Drug Deliv. Sci. Technol. 80 (2023) 104153.
[48] S. Chakraborty, S. Saha, V.R. Dhanak, K. Biswas, M. Barbezat, G.P. Terrasid, A.K. Chakraborty, High yield synthesis of amine functionalized graphene oxide and its surface properties, RSC Adv. 6 (2016) 67916–67924.
[49] B.O. Isiuku, P.C. Okonkwo, C.D. Emeagwara, Batch adsorption isotherm models applied in single and multicomponent adsorption systems–a review, J. Dispersion Sci. Technol. 42 (12) (2021) 1879–1897.
[50] J. Ma, C. Wang, W. Xi, Q. Zhao, S. Wang, M. Qiu, J. Wang, X. Wang, Removal of radionuclides from aqueous solution by manganese dioxide-based nanomaterials and mechanism research: a review, ACS ES&T Eng. 1 (4) (2021) 685–705.
[51] R.T. Yang, S.J. Doong, Gas separation by pressure swing adsorption: a pore-diffusion model for bulk separation, AIChE J. 31 (11) (1985) 1829–1842.
[52] M. Haghighi, A. Khoshfetrat, Au-O-MWCNTs and TiO2-O-MWCNTs as efficient nanocarriers for dexamethasone: adsorption isotherms and kinetic studies, Int. J. Chem. Eng. 2021 (2021).
[53] M.M. Dubinin, The potential theory of adsorption of gases and vapors for adsorbents with energetically nonuniform surfaces, Chem. Rev. 60 (1960) 235–241.
[54] J.A. Ramos-Guivar, K. Taipe, M.A. Schettino Jr., E. Silva, M.A.M. Torres, E.C. Passamani, F.J. Litterst, Improved removal capacity and equilibrium time of maghemite nanoparticles growth in zeolite type 5a for Pb (II) adsorption, Nanomater. 10 (9) (2020) 1668.
[55] J. Wang, X. Guo, Adsorption isotherm models: classification, physical meaning, application and solving method, Chemosphere 258 (2020) 127279.
[56] A.A. Noyes, W.R. Whitney, The rate of solution of solid substances in their own solutions, J. Am. Chem. Soc. 19 (1897) 930-934.

[57] R.W. Korsmeyer, R. Gurny, E. Doelker, P. Buri, N.A. Peppas, Mechanisms of solute release from porous hydrophilic polymers, Int. J. Pharm. 15 (1) (1983) 25–35.
[58] T. Higuchi, Rate of release of medicaments from ointment bases containing drugs in suspension, J. Pharmacol. Sci. 50 (10) (1961) 874–875.
[59] A.W. Hixson, J.H. Crowell, Dependence of reaction velocity upon surface and agitation, Ind. Eng. Chem. 23 (1931) 923–931.
[60] M.L. Bruschi, Strategies to Modify the Drug Release from Pharmaceutical Systems, Mathematical models for drug release, Chapter 5 (2015) 63–86.
[61] K. Wang, J. Pang, L. Li, S. Zhou, Y. Li, T. Zhang, Synthesis of hydrophobic carbon nanotubes/reduced graphene oxide composite films by flash light irradiation, Front. Chem. Sci. Eng. 12 (2018) 376–382.
[62] Z. Yang, J. Liu, J. Liu, X. Chen, T. Yan, Q. Chen, Investigation on physicochemical properties of graphene oxide/nano-hydroxyapatite composites and its biomedical applications, J. Aust. Ceram. 57 (2) (2021) 625–633.
[63] O.K. Taghzouti, K.E. Mabrouk, M. Bricha, K. Nouneh, Controlled adsorption and release of amoxicillin in GO/HA composite materials, SN Appl. Sci. 1 (3) (2019) 226.
[64] S.M. Prabhu, A. Khan, M.H. Farzana, G.C. Hwang, W. Lee, G. Lee, Synthesis and characterization of graphene oxide-doped nanohydroxyapatite and its adsorption performance of toxic diazo dyes from aqueous solution, J. Mol. Liq. 269 (2018) (2018) 746–754.
[65] A. Ślósarczyk, Z. Paszkiewicz, C. Paluszkiewicz, FTIR and XRD evaluation of carbonated hydroxyapatite powders synthesized by wet methods, J. Mol. Struct. 744–747 (2005) 657–661, 2005.
[66] S. Chakraborty, S. Saha, V.R. Dhanak, K. Biswas, M. Barbezat, G.P. Terrasid, A.K. Chakraborty, High yield synthesis of amine functionalized graphene oxide and its surface properties, RSC Adv. 6 (72) (2016) 67916.
[67] A. Olad, H.B.K. Hagh, Graphene oxide and amin-modified graphene oxide incorporated chitosan-gelatin scaffolds as promising materials for tissue engineering, Compos. B Eng. 162 (2019) 692–702.
[68] S. Oktay, N. Alemdar, Electrically controlled release of 5-fluorouracil from conductive gelatin methacryloyl-based hydrogels, J. Appl. Polym. Sci. 136 (1) (2019) 46914.
[69] N.A. Rangel-Vázquez, D.N. Villanueva-García, J. Kalla, Structural analysis of adsorption processes of 5FU and imiquimodon hydrogels using AMBER/PM3 hybrid model, Rev. Colomb. Quím. 47 (2) (2018) 28–35.
[70] F. Absalan, M.S. Sadjadi, N. Farhadyar, M.H. Sadr, Synthesis and characterization of mesoporous HA/GO nanocomposite in the presence of chitosan as a potential candidate for drug delivery, Chem. Pap. 75 (9) (2021) 4565–4578, 2021.
[71] J. Cui, J. Li, H. Qiu, G. Yang, S. Zheng, J. Yang, Zwitterionic graphene oxide modified with two silane molecules for multiple applications, Chem. Phys. Lett. 706 (2018) 543–547, 2018.
[72] M. Tourbin, F. Brouillet, B. Galey, N. Rouquet, P. Gras, N.A. Chebel, D. Grossin, C. Frances, Agglomeration of stoichiometric hydroxyapatite: impact on particle size distribution and purity in the precipitation and maturation steps, Powder Technol. 360 (2020) 977–988.
[73] A.R. Ibrahim, X. Li, Y. Zhou, Y. Huang, W. Chen, H. Wang, J. Li, Synthesis of spongy-like mesoporous hydroxyapatite from raw waste eggshells for enhanced dissolution of ibuprofen loaded via supercritical CO2, Int. J. Mol. Sci. 16 (4) (2015) 7960–7975.
[74] S.N. Ahmed, W. Haider, Enhanced photocatalytic activity of ZnO-graphene oxide nanocomposite by electron scavenging, Catalysts 11 (2) (2021) 187.
[75] R.S. Antônio, A.C.S. Guerra, M.B. de Andrade, L. Nishi, A.T.A. Baptista, R. Bergamasco, A.M.S. Vieira, Application of graphene nanosheet oxide for atrazine adsorption in aqueous solution: synthesis, material characterization, and comprehension of the adsorption mechanism, Environ. Sci. Pollut. Res. 28 (2021) 5731–5741.
[76] S. Mondal, M.E. De Anda Reyesa, U. Pal, Plasmon induced enhanced photocatalytic activity of gold loaded hydroxyapatite nanoparticles for methylene blue degradation under visible light, RSC Adv. 7 (14) (2017) 8633–8645.
[77] R.A. Almotiri, M.M. Alkhamisi, Physico-chemical behavior and microstructural manipulation of nanocomposites containing hydroxyapatite, alumina, and graphene oxide, Appl. Phys. A: Mater. Sci. Process. 128 (2022) 351.
[78] B. Nataraju, E. Kalenius, T. Udayabhaskararao, T. Pradeep, Ha Siegenthaler, T. Wandlowski, Phase transfer induced enhanced stability of monolayer protected silver quantum clusters, J. Clust. Sci. 29 (2018) 41–48.
[79] P.C. Mukesh Kumar, K. Palanisamy, V. Vijayan, Stability analysis of heat transfer hybrid/water nanofluids, Mater. Today: Proc. 21 (2020) 708–712.
[80] J. Kamieniak, P.J. Kelly, C.E. Banks, A.M. Doyle, Mechanical, pH and thermal stability of mesoporous hydroxyapatite, J. Inorg. Organomet. Polym. Mater. 28 (1) (2018) 84–91.
[81] C.H. Nguyen, C.C. Fu, Z.H. Chen, T.T.V. Tran, S.H. Liu, R.S. Juang, Enhanced and selective adsorption of urea and creatinine on amine-functionalized mesoporous silica SBA-15 via hydrogen bonding, Microporous Mesoporous Mater. 311 (2021) 110733.
[82] J. Wielińska, A. Nowacki, B. Liberek, 5-fluorouracil-complete insight into its neutral and ionised forms, Molecules 24 (20) (2019) 3683.
[83] K. Mioduszewska, J. Dołżonek, D. Wyrzykowski, Ł. Kubik, P. Wiczling, C. Sikorska, M. Toński, Z. Kaczyński, P. Stepnowski, A. Białk-Bielińska, Overview of experimental and computational methods for the determination of the pKa values of 5-fluorouracil, cyclophosphamide, ifosfamide, imatinib and methotrexate, TrAC, Trends Anal. Chem. 97 (2017) 283–296.
[84] M. Simeonova, R. Velichkova, G. Ivanova, V. Enchev, I. Abrahams, Poly(butylcyanoacrylate) nanoparticles for topical delivery of 5-fluorouracil, Int. J. Pharm. 263 (1–2) (2003) 133–140.
[85] M. Toński, J. Dołżonek, M. Paszkiewicz, J. Wojsławski, P. Stepnowski, A. Białk-Bielińska, Preliminary evaluation of the application of carbon nanotubes as potential adsorbents for the elimination of selected anticancer drugs from water matrices, Chemosphere 201 (2018) 32–40.
[86] T.A. Khan, S. Dahiya, I. Ali, Use of kaolinite as adsorbent: equilibrium, dynamics and thermodynamic studies on the adsorption of Rhodamine B from aqueous solution, Appl. Clay Sci. 69 (2012) 58–66.
[87] S. Yildiz, Kinetic and isotherm analysis of Cu (II) adsorption onto almond shell (Prunus Dulcis), Ecol. Chem. Eng. S 24 (2017) 87–106.
[88] H.M. El-Zeiny, M.R. Abukhadra, O.M. Sayed, A.H.M. Osman, S.A. Ahmed, Insight into novel β-cyclodextrin-grafted-poly (N-vinylcaprolactam) nanogel structures as advanced carriers for 5-fluorouracil: equilibrium behavior and pharmacokinetic modeling, Colloids Surfaces A Physicochem. Eng. Asp. 586 (2020) 124197.
[89] M.R. Abukhadra, N.M. Refay, A.M. El-Sherbeeny, M.A. El-Meligy, Insight into the loading and release properties of MCM-48/biopolymer composites as carriers for 5-Fluorouracil: equilibrium modeling and pharmacokinetic Studies, ACS Omega 5 (20) (2020) 11745–11755.
[90] X. Wang, J. Xu, X. Xie, X. Li, Z. Liu, Poly(vinyldiaminotriazine) nanoparticle adsorption of small drug molecules in aqueous phase and the role of synergistic interaction between hydrogen bonding and hydrophobic affinity, Colloid Polym. Sci. 299 (2021) 37–47.
[91] M.R. Abukhadra, A.A. AlHammadi, J.S. Khim, J.S. Ajarem, A.A. Allam, M.S. Shaban, Enhanced adsorption and visible light photocatalytic removal of 5-Fluorouracil residuals using environmental NiO/geopolymer nanocomposite: steric, energetic, and oxidation studies, J. Environ. Chem. Eng. 10 (6) (2022) 108569.
[92] S. Kar, B. Kundu, R.L. Reis, R. Sarkar, P. Nandy, R. Basu, S. Das, Curcumin ameliorates the targeted delivery of methotrexate intercalated montmorillonite clay to cancer cells, Eur. J. Pharmaceut. Sci. 135 (2019) 91–102.
[93] M.L. Laracuente, M.H. Yu, K.J. McHugh, Zero-order drug delivery: state of the art and future prospects, J. Control. Release. 327 (2020) 834–856.
[94] M.M. Ghobashy, A.M. Elbarbary, Dalia E. Hegazy, Gamma radiation synthesis of a novel amphiphilic terpolymer hydrogel pH-responsive based chitosan for colon cancer drug delivery, Carbohydr. Polym. 263 (2021) 117975.
[95] K.M. Sahu, A. Biswal, U. Manisha, Sarat K. Swain, Synthesis and drug release kinetics of ciprofloxacin from polyacrylamide/dextran/carbon quantum dots (PAM/Dex/CQD) hydrogels, Int. J. Biol. Macromol. 269 (2024) 132132.
[96] G. Bharath, K. Rambabul, F. Banat, S. Anwer, S.M. Lee, N.B. Saleh, S. Latha, N. Ponpandian, Mesoporous hydroxyapatite nanoplate arrays as pH-sensitive drug carrier for cancer therapy, Mater. Res. Express 6 (8) (2019) 085409.
[97] D. Feng, J. Shi, X. Wang, L. Zhanga, S. Cao, Hollow hybrid hydroxyapatite microparticles with sustained and pH-responsive drug delivery properties, RSC Adv. 47 (3) (2013) 24975–24982.

[98] B.K. Heragh, S. Javanshir, G.R. Mahdavinia, M.R. Naimi-Jamal, Development of pH-sensitive biomaterial-based nanocomposite for highly controlled drug release, Results Mater 16 (2022) 100324.
[99] G. Bharath, B.S. Latha, E.H. Alsharaeh, P. Prakash, N. Ponpandian, Enhanced hydroxyapatite nanorods formation on graphene oxide nanocomposite as a potential candidate for protein adsorption, pH controlled release and an effective drug delivery platform for cancer therapy, Anal. Methods 9 (2) (2017) 240–252.
[100] S. Rakass, H.O. Hassani, A. Mohmoud, F. Kooli, M. Abboudi, E. Assirey, F. Al Wadaani, Highly efficient methylene blue dye removal by nickel molybdate nanosorbent, Molecules 26 (5) (2021) 1378.
[101] V.K. Garg, R. Gupta, A.B. Yadav, R. Kumar, Dye removal from aqueous solution by adsorption on treated sawdust, Bioresour. Technol. 89 (2) (2003) 121–124.
[102] A.S. Alzaydien, Adsorption behavior of methyl orange onto wheat bran: role of surface and pH, Orient, J. Chem. 31 (2) (2015) 643–651.
[103] M. Vall, P. Zhang, A. Gao, S. Frykstrand, O. Cheung, M. Strømme, Effects of amine modification of mesoporous magnesium carbonate on controlled drug release, Int. J. Pharm. 524 (1–2) (2017) 141–147.
[104] M. Pishnamazi, H. Hafizi, M. Pishnamazi, A. Marjani, S. Shirazian, G.M. Walker, Controlled release evaluation of paracetamol loaded amine functionalized mesoporous silica KCC1 compared to microcrystalline cellulose based tablets, Sci. Rep. 11 (2021) 535.
[105] M. Tang, S. Liu, L. Luo, F. Cao, C. Wang, R. Chen, J. Shen, Synthesizing surface modified hydroxyapatite embedded in three-dimensional graphene oxide networks for drug loading, Mater. Lett. 265 (2020) 127426.
[106] E. Murugan, C.R. Akshata, Graphene oxide reinforced SrHAP composite as a drug carrier in bone regeneration, Colloids Surf. B Biointerfaces 219 (2022) 112822.